Final Design Report: BIA

Ankle-Foot Orthosis (AFO) Design

Project Advisor:

Dr. Paul Labossiere, P. Eng.

Sponsoring Company:

Anderson Orthopedics

Submission Date:

Wednesday, December 7, 2016

PREPARED BY:

TEAM 1

AFOT

FRANZESKA HEMPEL   ZAFAR JAVED   CHANELLE MCKENZIE   MISILYNA WU

Executive Summary

The team was assigned to work with Anderson Orthopedics (AO), a private company specializing in the ability to provide patients with a customized ankle-foot orthosis (AFO). The main objective of the project was to optimize the posterior strut geometry of the AFO for individuals suffering from dorsiflexor and plantarflexor weaknesses, and be able to 3D print the brace in order to receive patient feedback.

After identifying the needs and constraints of the project, the team was able to begin concept development for the AFO and brainstormed 17 preliminary concepts, which were narrowed down to four concepts using qualitative screening analyses. The top four designs chosen were: the Basic (#1), Wishbone (#5), Posterior Lattice (#10), and Layered Strut (#11) concepts. Finally, a preliminary qualitative FEA scoring analyses was performed in order to choose the final concept design to further optimize based on the performances under the constrained settings of the gait cycle, on a modifying software SolidWorks®. As a result, the Basic concept was selected.

In order to optimize the design of the Basic concept, the team considered three main variables: material selection, inclination angle, and material thickness. The final model chosen to 3D print was made out of PC-ISO and an inclination angle of 90°, which we name the Basic (PC-ISO, 90°). Using this model, further optimization and customization of the brace was performed, which resulted in the final model: BIA.

The BIA was 3D printed using PC-ISO at an inclination angle of 90°, sole thickness of 3 mm, and varying posterior strut thickness from 4-7 mm, which resulted in a spring-back force of approximately 168 N, and an estimated increase in energy return of 38%. The total cost of manufacturing the BIA at North Forge was roughly $264.

The last phase of the project consisted of 3D printing the Basic (PC-ISO, 90°) model and presenting our final model, BIA, to the client and patient for feedback. After receiving feedback from both the client and patient, recommendations for any future development in the project were made.

TABLE OF CONTENTS

List of Figures

List of Tables

Glossary

Abbreviation	Meaning
N/A	Not Applicable
NA	Not Available
S-N Curve	A plot of stresses (S) against the number of cycles until failure (N)

Acronym	Description
AFO	ankle-foot orthosis
AO	Anderson Orthopedics
CAD	computer-aided design
COTS	commercial off-the-shelf
E	elastic modulus*
EB	elongation at break*
FS	fracture strength*
FEA	Finite element analysis
FMEA	failure modes and effects analysis
SF	safety factor
P&O	prosthetics and orthotics
SG	specific gravity*
T	temperature distortion*
TS	tensile strength*

* Indicates variables used in TABLE IX on page 20

Term	Definition
Client	William Hadi, the primary contact at Anderson Orthopedics
Final Concept	The highest ranked preliminary concept, determined using screening, scoring, and preliminary FEA
Final Model	The highest ranked concept modelled using SolidWorks® after optimization
Final Product	The final 3D printed AFO tested by the patient

Heel Cup	The region of the AFO that supports the heel, and connects the posterior strut to the sole
Orthopedic	A branch of medicine focused on the correction of deformities of bones and/or muscles [1]
Orthosis	Medical braces used to provide support or correct alignment of limbs and/or spines [2]
Patient	The individual who volunteered to test the final product
Posterior Strut	The section of the AFO that lies along the calf of an individual, creating a bridge between the sole of the AFO and the point of attachment
Preliminary Concept	A conceptual design created by the team members during concept generation
Prosthesis/Prosthetic	An artificial device used to replace and mimic the function of the missing internal or external body part of an individual [3]

1.0 INTRODUCTION

Anderson Orthopedics (**AO**) was founded in Winnipeg, Manitoba in 1945 as a private prosthetic provider [4]. In the past 71 years, the company has expanded and now specializes in prosthetics and orthotics, helping everyone from pediatric to geriatric patients who suffer from missing limbs and reduced mobility. AO has branched out and currently provides additional clinical services in Brandon and The Pas, becoming an industry leader within the province. The company consists of a group of certified prosthetists and orthotists who work together to provide customized upper and lower limb prosthetics, as well as upper limb, lower limb and spinal orthoses. Currently, the company designs and manufactures each specialized product with a combination of materials, including polypropylene plastics, metals, carbon fibre, and a variety of composites. The company is working towards utilizing more quantitative measures to dictate the design of the devices and more accurately assess their effectiveness and influence on the final clinical outcome. Additionally, AO is interested in exploring the feasibility of 3D printing prosthetics and orthotics. The first step towards AO achieving this goal was to investigate the feasibility of optimizing the current ankle-foot orthosis (**AFO**) design.

The team was sponsored by and worked together with AO to optimize the posterior strut geometry of an AFO. The team was given the opportunity to develop an AFO model that could provide an optimal amount of forward propulsion and could be 3D printed. As a result, the team developed and manufactured a model, named the BIA. The word "bia" was chosen as the name for the final product because it represents force, power, bodily strength, and raw energy in Greek mythology [5].

The BIA was modeled and manufactured to reduce the amount of material around an individual's leg and eliminate material buckling around the ankle. The BIA was modelled using SolidWorks® and analyzed using Finite element analysis (**FEA**). The design was tested at three different angles with three different materials to determine the most suitable design, which consisted of an inclination angle of 90° and a material of PC-ISO plastic. The final model was further optimized, in order to

increase the spring-back force provided to the patient, by varying the thickness of different sections of the brace. The design of the BIA met the two main design needs of the client by providing 168N of spring-back force, which was an increase of 38% compared to the commercial off-the-shelf (**COTS**) AFO, and by being manufactured and tested by one of the patients at AO. The report provides an explanation of the methodology and analysis that was performed to finalize the design.

1.1 Background

An AFO is primarily used to aid individuals who suffer from a weakness in dorsiflexor muscles. It is common for an individual who suffers from a weakness in his/her dorsiflexor muscles to also suffer from weaknesses in the opposing plantarflexor muscles [6]. Dorsiflexion is the motion of lifting the toes towards the shin, while plantarflexion is the motion of pointing the toes away from the shin, as shown in Figure 1 [7].

Figure 1. Engagement of the dorsiflexor and plantarflexor muscles when lifting the toes upward and pointing the toes towards the ground, respectively [6].

Aggravation of the dorsiflexor and plantarflexor muscles can cause discomfort, resulting in challenges when walking. Every time a step is taken, the foot goes through two phases of motion: a stance phase, when the foot is on the ground, and a swing phase, when the foot is off the ground [7]. The dorsiflexor and plantarflexor

2

muscles work together by contracting simultaneously and independently at different stages of gait to produce a normal walking cycle, shown in Figure 2.
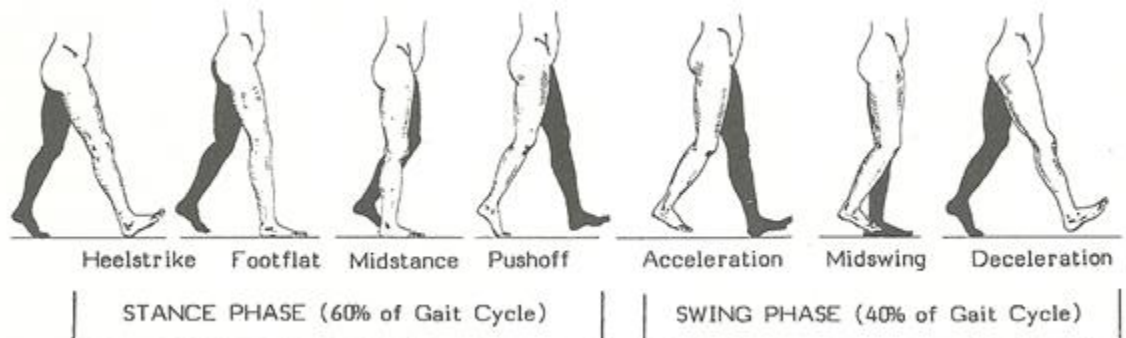
Figure 2. Gait cycle of an individual without any plantarflexion or dorsiflexion weakness separated into the stance phase and the swing phase [7].

In addition to the dorsiflexor muscles lifting the foot up during the swing phase, these muscles also help control plantarflexion after heel strike [7]. The combination of these two actions allows the foot to clear the ground during acceleration and prepare for the next step. The primary role of the plantarflexor muscles are to help the foot push off the ground and propel an individual forward, by the end of the stance phase.

Weakness in the dorsiflexor and plantarflexor muscles can stem from medical conditions, such as strokes, multiple sclerosis, spina bifida, cerebral palsy, and other upper and lower motor neuron related pathologies. When an individual suffers from a weakness in his/her dorsiflexor muscles, he/she may display a gait pattern where the sole of the foot slaps uncontrollably against the ground at the point of heel strike [8]. Additionally, the distal part of the individual's foot catches along the ground during the pre-swing phase. As a result, these individuals are prone to tripping frequently. If a supportive brace is not worn, the flex at the hip and knee tend to become exaggerated to prevent the foot from catching on the ground. Plantarflexion weakness can generally result in difficulties for an individual to propel his/her foot and body forward.

For an individual with both dorsiflexor and plantarflexor muscle weaknesses, an AFO is utilized to improve his/her gait cycle. The design of an AFO provides forward propulsion to the foot at the end of the stance phase, and supports the foot during the swing phase. The forward propulsion of the orthosis is created by the posterior strut of the AFO, which acts as a spring [8]. The energy providing the forward propulsion comes from a transfer of potential to kinetic energy. The potential energy is stored in the brace during the stance phase as the brace dorsiflexes; that energy is then transferred to kinetic energy as the brace springs back to its neutral position when the foot lifts off the ground, providing a plantarflexion moment. The magnitude of this moment can be optimized by modifying the geometry of the posterior strut and the material composition of the AFO.

An AFO is commonly made out of plastic and designed to dynamically support the ankle and foot with the ultimate goal of restoring the patient's gait, as much as possible, to that of the norm, while improving his/her safety while walking [9]. The orthosis slips underneath the sole of the foot and typically wraps around the back of the calf, bracing the foot in a flat position. A commercial off-the-shelf **(COTS)** AFO, shown in Figure 3, can be used by patients with a dorsiflexor weakness and a mild plantarflexor muscle weakness as long as their anatomy fits comfortably with the pre-fabricated design.

Figure 3. COTS AFO used to support plantarflexion and dorsiflexion weakness [10].

Although the COTS AFO is available to all individuals, those who have a severe case of plantarflexor and dorsiflexor muscle weakness require more propulsion. As a result, AO provides custom AFOs to increase the amount of the plantarflexion moment the brace generates. AO is able to cater to various patients by optimizing the AFO geometry to meet the needs of each individual.

AO focuses on meeting each individual's needs by customizing the angle of the brace at the ankle in addition to the posterior strut design. The customization process begins by replicating the geometry of an individual's lower leg with a fiberglass cast, which is then 3D scanned [9]. The result of the scan is exported into Canfit™ Vorum **P&O CAD** software, which allows the orthotists to design a brace that will fit the shape of the individual's sole and calf. The software also allows some ability to shape the posterior strut of the AFO, with the goal of providing sufficient propulsion to the individual's foot to help simulate a natural gait cycle.

1.2 Problem Statement

AO is currently able to provide patients with custom plastic AFOs, as well as COTS plastic and carbon fibre AFOs. The company is working towards providing these patients with custom 3D printed AFOs. However, the current design is not compatible with the 3D printing manufacturing process, as the plastics available are too brittle to support the geometry. Additionally, in the current design of the AFO, the potential energy is not fully transferred to the forward propulsion of the foot, which in turn reduces the effectiveness of the brace.

1.3 Project Objective and Scope

The objective of the project was to optimize the design of the current plastic AFO model for 3D printing and to optimize the geometry of the posterior strut to increase forward propulsion at the push-off phase during the gait cycle. The team was not required to redesign the sole of the AFO or the method used to attach the AFO to the patient's leg.

In order to achieve these project objectives, the team was required to satisfy the following criteria within the time allotted to the design project:

i) The AFO designed can be manufactured using a 3D printer

ii) Redesign the posterior strut to optimize forward propulsion

iii) Redesign the heel cap to prevent material buckling

iv) Perform cyclic loading calculations to verify that the AFO can endure the required number of gait cycles

v) Stress analysis using FEA to ensure that the AFO can support the patient without fracturing or buckling

vi) Verify the amount of forward propulsion provided to the patient by using the virtual physics environment of SolidWorks®

vii) Design the final AFO concept within the budget provided by AO

The following deliverables were provided to AO at the end of the design project:

i) CAD models and drawings of the AFO design

ii) Virtual force results of the AFO's propulsion performance

iii) FEA of the AFO's structural performance

iv) Weight and design comparisons between a COTS AFO and the team's design

v) Complete project budget, based on the costs of local 3D printing facilities

If time permits, the team will also include the following deliverables in the project:

vi) 3D printed prototype of the team's final design

vii) Results from physical tests of the patient walking with the 3D printed AFO

2.0 DESIGN NEEDS ANALYSIS

Before the team could develop concepts to optimize the AFO, it was essential that the project needs, constraints and target specifications defined by the client, were identified. The team identified 19 needs and 13 constraints for the project, along with 27 metrics. The following section identifies and evaluates these needs and constraints, and establishes the metrics and preliminary target specifications.

2.1 Design Needs

A list of design needs for the AFO was compiled based on information and feedback from the client. The relative importance of these needs was analyzed and characterized by the team using a ranking system of 0-5 indicating an increasing order of importance. The needs were then categorized into three categories: functional, patient, and client specific needs. The results of this analysis are shown in TABLE I.

TABLE I
NEEDS IDENTIFIED BY THE CLIENT AND THEIR RELATIVE IMPORTANCE

	Need No.	Need	Description	Relative Importance
Functional	N1	AFO provides dorsiflexion and plantarflexion support	Accommodate for patients with varying weaknesses	5
	N2	Posterior strut geometry of the AFO is optimized	Optimize forward propulsion	5
	N3	AFO is compatible with the fibular head	Avoid irritation to peroneal nerve, which lies on fibular head	5
	N4	AFO operates normally with repeated use	Can be worn over long time periods	5
	N5	AFO supports weight of the patient	Absorb impact of heel strike and forces applied during gait cycle	5
	N6	AFO is durable	Avoid corrosion, wear, and fracturing	5
	N7	AFO is compatible with footwear	Fits inside patient's shoe	4
	N8	AFO operates normally in Manitoba climates	Endure extreme range of climates throughout the year	3
Patient	N9	AFO is free of sharp edges	Prevent discomfort, especially when swelling occurs	5
	N10	AFO is comfortable	No extra material added where unnecessary	4
	N11	AFO is easily attachable and removable	Requires the same amount of time to put on or take off shoes	4
	N12	AFO is as light as or lighter than the COTS model	Manufactured out of less or lighter material	2
	N13	AFO is discreet	Not noticeable when worn	1
	N14	AFO is affordable	To manufacture and replace	1
Client	N15	AFO is 3D printable	Consider feasibility of 3D printing	5
	N16	AFO is manufactured in Winnipeg	Facility is located or can be replicated in Winnipeg	5
	N17	AFO is easily manufactured	Reduce labour time and complexity	4
	N18	AFO helps patient simulate a natural gait cycle	Reduce compensation of other body parts (knee or hip)	4
	N19	AFO avoids buckling and warping during use	Eliminate material buckling around the ankle	2

After analyzing the ranking of needs in the project, the highest priority of this project was capability of the AFO to be 3D printed. A few other highly ranked needs included, the compatibility of the brace with the fibular head, the need to provide muscular support, the optimization of the posterior strut geometry, and the need to support the weight of the patient. The team was able to conclude that the needs related to the safety of the patient were of higher importance and were incorporated throughout the design process of the BIA.

2.2 Project Constraints

Once the design needs of the project were determined, it was important to identify the existing constraints and their respective implications. A summary of the constraints and their respective limiting parameters are shown in TABLE II.

TABLE II
PROJECT CONSTRAINTS AND LIMITING PARAMETERS

No.	Constraint/Limitation	Limiting Parameter
C1	Heel support size	Dimensions of a standard running shoe
C2	Material selection	Materials that can be 3D printed
C3	Material testing	S-N curve
C4	Material properties	Yield strength
C5	Product evaluation	Mostly qualitative or subjective analysis has been performed, therefore assumptions are necessary to simplify analysis
C6	Environment	Extreme climates in Manitoba all-year-round
C7	Cast scanner	Spectra™ 3D Scanner (by Vorum)
C8	Modifying CAD software	Canfit™ Vorum P&O
C9	FEA CAD software	SolidWorks®
C10	3D printer model	Available in North Forge Fabrication Lab
C11	3D printing capabilities	Direction and orientation of material printing
C12	Cost	$700 (including materials and labour)
C13	Time	September 14, 2016 – December 8, 2016 (85 days)

Once these 13 project constraints and their limiting parameters were identified, target specifications for each of the 17 needs were developed and compared with 27 metrics that were defined.

2.3 Design Metrics and Target Specifications

After presenting the design needs and constraints of the project, a minimum of one metric was selected to evaluate whether or not a design successfully met the needs. The relative importance of these metrics was evaluated using the same method as the needs in TABLE I. The appropriate units were assigned to each metric in order to specify the type of evaluation conducted. Finally, preliminary target specifications were assigned to each metric based on the information provided by the client and the COTS AFO benchmark. The results of the metric and preliminary target specifications are shown in TABLE III.

TABLE III
METRICS AND PRELIMINARY TARGET SPECIFICATIONS

			Metric	Target Specification	Unit	Relative Importance
Functional	N1	M1	Bending stress	NA	MPa	5
		M2	Spring-back force	NA	N	5
	N2	M3	Posterior strut thickness	4	mm	3
		M4	Posterior strut length	340	mm	3
		M5	Posterior strut width	30-104	mm	3
	N3	M6	Proximity of AFO to fibular head	< 30	mm	5
	N4	M7	Fatigue failure	50,000	cycles	3
	N5	M8	Impact stress	NA	MPa	3
	N6	M9	Fracture stress	NA	MPa	5
	N7	M10	Sole thickness	2.5	mm	4
		M11	Sole length	265	mm	4
		M12	Sole width	95	mm	4
	N8	M13	Operating temperature range	-40 to 40	°C	3
Patient	N9	M14	Dental floss test	pass	pass/fail	5
	N10	M15	Clearance from bones/thin skin	3-5	mm	4
		M16	Comfort	> 8/10	subj.	5
	N11	M17	Time to attach and remove AFO	< 10	s	5
	N12	M18	Weight of the AFO	125	g	3
	N13	M19	Discrete appearance	> 8/10	subj.	1
	N14	M20	Manufacturing cost	400	$	2
		M21	Material cost	300	$	2
Client	N15	M22	3D printable design	yes	yes/no	5
	N16	M23	Delivery time	20	weeks	4
	N17	M24	Manufacturing time	< 50	hours	3
	N18	M25	Levelness of walk	NA	°	3
		M26	Instills dignity	> 8/10	subj.	2
	N19	M27	Buckling stress	NA	MPa	1

The metrics that did not have a target specification were labelled as **NA** (Not Available) and mainly, related to the functional needs that vary between patients.

3.0 FINAL PRELIMINARY DESIGN: BASIC CONCEPT

Once the needs, constraints, and specifications were understood, the team generated 17 concepts that would satisfy the needs of the client and the patient. The 17 concepts were narrowed down to the top four most optimal concepts using qualitative analysis, by combining similar concepts, and using screening and scoring matrices. A step-by-step methodology regarding how the team selected and weighted each criterion can be found in Appendix A. The top four concepts, the Basic, Wishbone, Posterior Lattice, and Layered Strut concept were further analyzed by performing qualitative FEA. The following section includes the preliminary FEA performed on each of the four concepts, resulting in the selection of the Basic concept as the most ideal final design, in terms of the patient and client needs.

3.1 Preliminary FEA

The main objective of performing FEA on each concept was to gage which of the top four concepts would be most suitable to support a foot with plantarflexion and dorsiflexion weakness. At this stage in the design, the team decided that the best method to analyze the concepts with FEA was to use an analytical approach, in contrast to a numerical approach. To evaluate each set of FEA results, only the posterior strut displacement and high stress areas were inspected. The results of each simulation was then scored to determine which posterior strut design had the greatest potential of supporting a load without failing. To ensure that the only changing variable from one design to another was the posterior strut geometry, design constraints were set while modeling. The overall dimensions of each concept were held constant to the dimensions of the COTS AFO. These dimensions were chosen as the constraint for each concept since the COTS AFO has proven to support a variety of individuals who experience weaknesses in the plantarflexor and dorsiflexor muscles. Therefore, these dimensions were able to provide insight into whether the final concept would be capable of supporting an individual just as well

as the COTS can before optimization takes place. In addition, the material of each concept was set as a constant to match the material of the COTS AFO. These constants are summarized in TABLE IV.

TABLE IV
DIMENSION AND MATERIAL CONSTRAINTS APPLIED TO THE BASIC, WISHBONE, POSTERIOR LATTICE AND LAYERED STRUT CONCEPTS DURING MODELING

Description	Dimension Value
Posterior strut height	340 mm
Posterior strut thickness	4 mm
Posterior strut width at upper calf	104 mm
Sole length	265 mm
Sole thickness	2.5 mm
Sole heel width	40 mm
Material	Homopolymer Polypropylene

It should be noted that the dimensions and material listed in TABLE IV were preliminary constraints to ensure a fair displacement comparison basis. These dimensions and material will be taken into consideration during the final optimization, but will not limit the optimization of the final concept. From these design constraints the Basic, Wishbone, Posterior Lattice, and Layered Strut concepts were modeled in SolidWorks®. The side and back view of each concept is illustrated in Figure 4 through Figure 7.

(side)   (back)
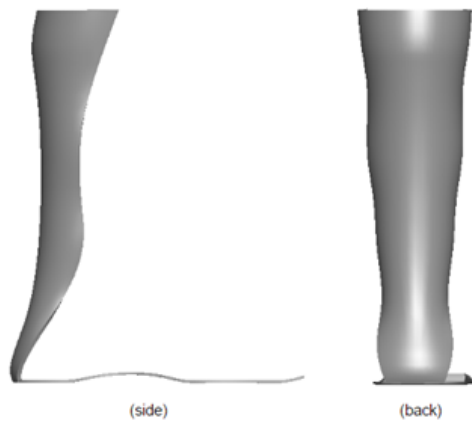
Figure 4. Side and back view of the modeled design of the Basic concept.

2
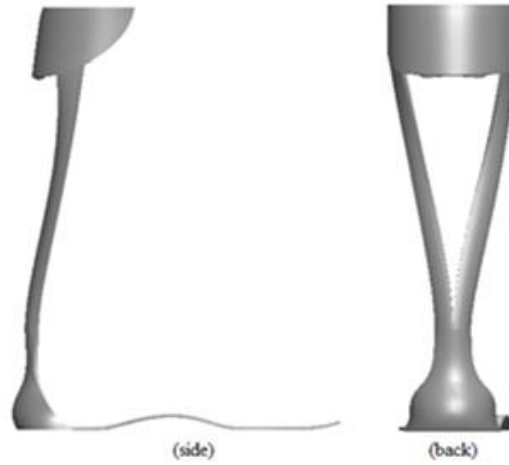
Figure 5. Side and back view of the modeled design of the Wishbone concept.
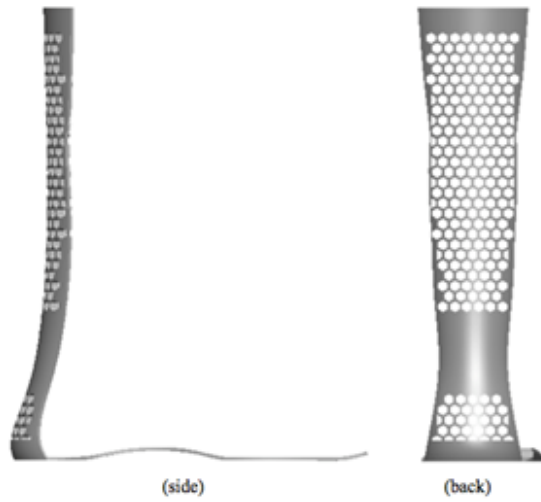
Figure 6. Side and back view of the modeled design of the Posterior Lattice concept.
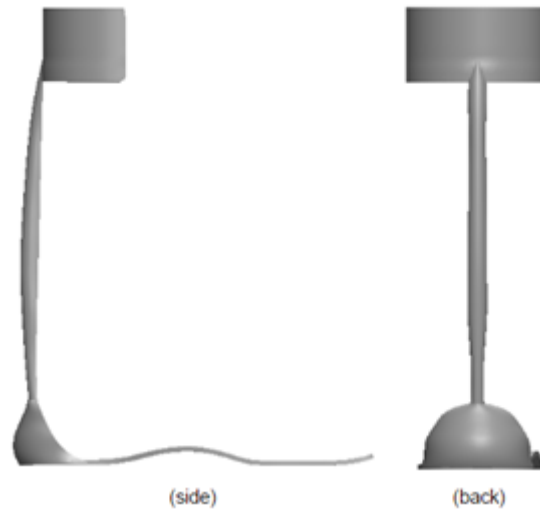
Figure 7. Side and back view of the modeled design of the Layered Strut concept.

Once modelled, each of the four concepts were simulated in FEA. The following section discusses how the constant applied force was calculated, the location of the forces, the mesh chosen, and the results of the FEA.

3.1.1.1 REACTION FORCE APPLIED TO AFO

One of the forces an AFO must endure is the force of an individual's leg pulling the posterior strut forward at the location of attachment around the calf. This force is applied every time a step forward is taken and is the greatest at the instance before the heel comes off the ground. As this force compresses the AFO, the posterior strut tries to spring back to its original geometry gradually. The forward pull of this force causes the posterior strut to flex and displace. Therefore, the force applied at the upper calf was calculated to add an additional constraint to the FEA simulation. This again ensures that the displacement of each posterior strut is comparable.

The posterior strut transfers potential energy into kinetic energy through the elastic properties of the AFOs material. Therefore, an AFO performs as a linear elastic model when it is compressed and released with each step. With this taken into consideration, the force applied to the posterior strut was calculated by assuming the posterior strut performs as a beam in bending, with one end fixed to the sole and with a load applied at the point of attachment around the calf. Figure 8 illustrates an

outline of the AFO in the stance position, the location of the force applied, the moment in the gait cycle right before the heel comes off the ground, and the distance that the AFO displaces based on the length of the posterior strut and the angle of deflection.
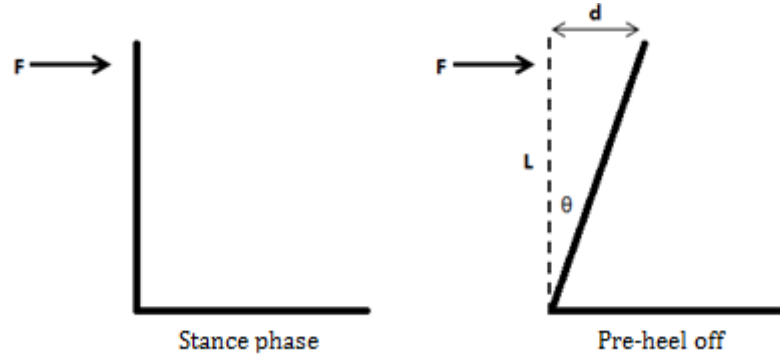
Figure 8. AFO outline of the stance phase pre force applied and the outline of an AFO post force applied and pre heel off.

Assuming the posterior strut performs as a linear elastic beam, the force applied to the AFO is directly proportional to the distance that it displaces. Therefore, the force used in the FEA simulation was calculated using equation (1).

$$F = kx \qquad (1)$$

In equation (1), k represented the stiffness of the material and was calculated using equation (2).

$$k = \frac{3EI}{L^3} \qquad (2)$$

In equation (2), E represented the elastic modulus of homopolymer polypropylene, E = 1790 MPa, provided by the material properties listed in SolidWorks®. L is the height of the posterior strut outlined in TABLE IV and the variable I represents the second moment of inertia relative to the dimensions in TABLE IV and equation (3).

$$I = \frac{bh^3}{12} \qquad (3)$$

The second moment of inertia of a beam in bending is based on the load applied to the cross sectional area. The highlighted area in Figure 9 illustrates this cross

5

sectional area. Labels b and h correspond to the width and height of the posterior strut dimensions outlined in TABLE IV.
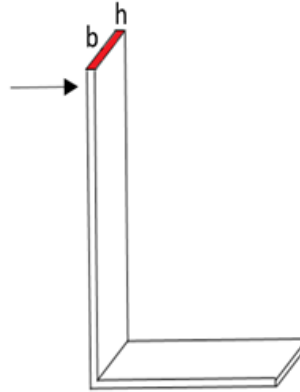
Figure 9. Highlighted cross sectional area considered when calculating the second moment of area of a beam under bending when a load is applied.

The preliminary calculations were analyzed using a rectangular posterior strut cross section, as shown in Figure 9. Although this geometry was different from those illustrated in Figure 4 through Figure 7, the calculation performed with the simplified geometry was considered so that a constant force could be applied to each concept. This calculation was later refined to more accurately reflect the geometry of the final concept.

Lastly, the only unknown variable in equation (1) was the distance that the AFO deflected from the neutral position, shown in Figure 9. Since the main purpose of an AFO is to replicate a natural gait cycle, the degree to which the AFO deflects should be proportional to the distance a healthy individual can lower his/her shin towards the top of the foot without bending the knee or raising the heel off the ground. This is known as the maximum dorsiflexion angle [11]. Once the foot reaches the maximum dorsiflexion angle, the heel of the foot naturally pops off the ground. For a healthy individual, this normally occurs at 20 degrees from the vertical position of the leg when standing. Therefore, for an individual who is unable to raise his/her heel off the ground, the AFO can help induce a spring back moment at 20 degrees to provide a natural gait cycle. By defining the value of theta to be 20°, as shown in

6

Figure 8, the resulting distance the AFO must be displaced was calculated using equation (4).

$$d = L \tan \theta \qquad (4)$$

TABLE V summarizes the results of equations (1), (2), (3) and (4).

TABLE V
EQUATIONS REQUIRED TO CALCULATE FORCE APPLIED TO THE MODEL AND
CORRESPONDING RESULTS

Equation Number	Equation	Result
(1)	$F = kx$	9.03 N
(2)	$k = \dfrac{3EI}{L^3}$	72.82 N/m
(3)	$I = \dfrac{bh^3}{12}$	5.33×10^{-4} m^4
(4)	$d = L \tan \theta$	0.124 m

The results of equation (2) provide a value for how much force must be applied to deflect a beam 20 degrees, if it had the same dimensions, material and geometry constraints as the COTS AFO. This force can now be used as a constant force on each of the four concepts to evaluate how the different posterior strut geometries react to the same load.

3.1.1.2 FEA BOUNDARY CONDITIONS

Since SolidWorks® is a CAD program with FEA capabilities, it does not have the same functionality as other FEA programs. In order to apply the FEA capabilities of SolidWorks®, the software requires that geometric constraints be applied to a design. This allows for the fixed geometry of the AFO and the applied forces acting on the posterior strut to be simulated. These forces were then evaluated within the constructed mesh along the AFO.

Fixture

For the FEA simulation, a fixed geometry was applied to the bottom of the AFO sole, in order to simulate the action of the pre-heel off stance, as shown in Figure 10. With this constraint defined, only the posterior strut deflected when a force was applied.
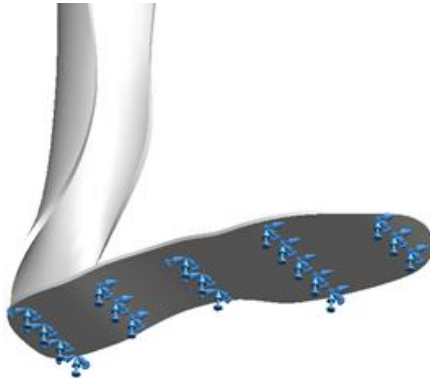
Figure 10. The bottom of the sole was used as a fixed geometry before the running the FEA.

The blue arrows shown in Figure 10 highlight the location of the fixed points along the sole of the AFO.

External loads

A force of 9.03 N was applied at the point of attachment around the calf. This location was chosen as the point of application since a Velcro strap wraps around the AFO and the individual's calf. As the individual steps forward, the strap around his/her leg applies a force to the back of the orthosis, causing the brace to flex. Figure 11 shows where the Velcro strap is located by highlighting the forces applied on the AFO by the strap.
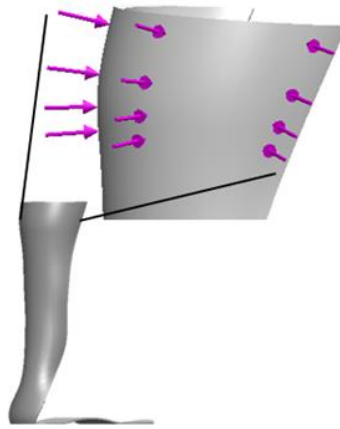
Figure 11. The arrows in the zoomed in view shows the forces applied at the point of attachment around the calf.

Meshing

In order to perform FEA, applying a mesh was required. By default, SolidWorks®
breaks up the structure into tetrahedral shapes, when meshing, with four nodes
with three degrees of freedom. Using these tetrahedrals, the reactions between each
node was approximated. Figure 12 shows the basic mesh that was initially applied
to the design.

Figure 12. Basic meshing of AFO design.

The mesh controls within FEA uncover any high or low stress concentration areas. Depending on the model being analyzed, the mesh may need to be reduced to a finer mesh or increased to a coarser mesh to provide the optimal results. If each of the four concepts was left at an unspecified mesh, the severity of stress concentrations uncovered would vary from one result to another, and could not be compared accurately. Therefore, to reduce the ambiguity of the results, a constant mesh was applied to each simulation, as shown in Figure 13.
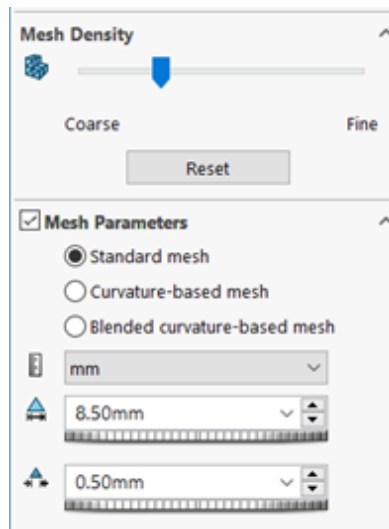
Figure 13. Mesh control settings used to evaluate the four concept AFO designs.
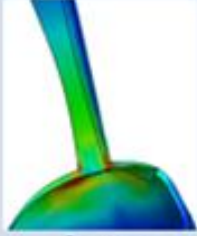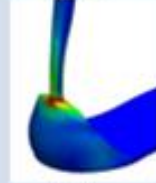
The maximum width of each tetrahedral was set to 8.5mm and the minimum width was set to 0.5 mm. Additionally, a standard mesh was applied to each design as a basic control for the preliminary analysis

3.1.1.3 FEA Results

After setting up the geometric constraints in SolidWorks®, FEA was performed on each concept.

TABLE VI compares the displacement results of each concept and highlights the high stress areas on each model.

TABLE VI
SIDE VIEW OF AFO DESIGN BEFORE AND AFTER FEA, HIGHLIGHTING AREAS OF
HIGH STRESS CONCENTRATION DUE TO LOADING AT POSTERIOR STRUT

As a reference, a colored gradient scale was included within the table, where red represents the regions of high stress and blue represents the regions of low stress. This scale represents the varying stresses the AFO experiences under the 9.03N load, and its values varied from 0 to 35.03MPa, the yield strength of homopolymer polypropylene [12]. The results of each model was analyzed to determine where the high stresses developed and the deformation that occurred to each design as the

stress was applied. The following summaries give further detail of the results of each model from the preliminary FEA.

Concept 1 – Basic

The FEA analysis of the Basic concept showed a linear displacement of the posterior strut forward, without any deformities to the overall shape of the orthosis. The high stress areas highlighted that the stress redistribution was very low at the connection between the heel and the sole of the AFO. With such low stress distributions throughout the model, this concept would have more potential for further optimization, as the current geometry was able to support the overall geometry change of an AFO during the pre-heel off phase of the gait cycle.

Concept 5 – Wishbone

The FEA of the Wishbone concept showed the displacement of the posterior strut to be very similar to that of the basic concept. The FEA shows the stress redistribution to be greatest around both the inner and outer region of the achilles heel. The higher stress in this area appears to cause the connection between the two struts to warp forward as the force is applied. As the highest stresses are located along the thinnest width and the edges of the design, the geometry of this concept would need to be optimized to better support the load applied to the posterior strut.

Concept 10 – Posterior Lattice

The FEA simulation of the Posterior Lattice concept showed the smallest displacement of the posterior strut in comparison to the other three concepts. The results of the FEA show two regions of high stress. The first is the region of the honeycomb wrapping around the back of the calf and the second is the edges along the honeycomb lattice. With such high stresses redistributions along the edge of the lattice structure, this concept could have been improved, if pursued. Both the lattice geometry and positioning could be analyzed further to optimize the design to better support the deflection of the AFO during the gait cycle.

Concept 11 – Layered Strut

The FEA of the Layered Strut concept showed the greatest displacement of the posterior strut. In comparison to the other FEA models this concept has the greatest stress redistribution around the heel. This was due to the sharp change in geometry from the large surface of the heel support to the reduced surface of the posterior strut. A localized stress concentration at the connection between the heel support and the posterior strut is not suitable for the application of an AFO. As a result, this concept would require redesigning before any form of optimization.

These four concepts were analyzed using a concept scoring process, in order to determine the final concept for the optimization phase of the design project.

3.1.2 Concept Scoring Analysis

The scoring process was set up such that each team member would evaluate each of the concepts in comparison to each other individually, and then the results would be compiled and discussed. The team decided that the scores should be evaluated based on a scale from zero to four, where zero indicated the lowest possible score and four represented the highest score. Although a score from zero to ten was a more typical range, it would be difficult to differentiate between various increments where a mere four concepts were being compared. Instead, the range selected corresponded to the number of concepts, such that there would be a clear hierarchy. The final results of this scoring process are shown in TABLE VII.

TABLE VII
SUMMARY OF THE SCORING ANALYSIS FOR EACH OF THE FINAL CONCEPTS

		Concept							
		#1 Basic		**#5 Wishbone**		**#10 Posterior Lattice**		**#11 Layered Strut**	
Criteria	**Weight**	**Rating**	**Score**	**Rating**	**Score**	**Rating**	**Score**	**Rating**	**Score**
Stress distribution	0.33	4	1.32	4	1.32	3	0.99	1	0.33
Prevalence of problem prone areas	0.17	4	0.68	3	0.51	3	0.51	2	0.34
Degree of displacement	0.17	4	0.68	4	0.68	4	0.68	2	0.34
Maintains shape	0.33	4	1.32	3	0.99	4	1.32	3	0.99
Total Score		4		3.5		3.5		2	
Rank		1		2		2		3	
Continue?		Y		N		N		N	

After scoring the four concepts, the Basic concept was ranked first, the Wishbone and Posterior Lattice concepts were ranked second, and the Layered Strut concept was ranked the lowest.

Once the Basic concept was chosen as the final concept, various optimizations were considered, such as the thickness of the posterior strut, the angle of the posterior strut, and the material selection. Although polypropylene was used for the preliminary FEA, other materials used by 3D printers were explored for further optimization.

4.0 FINAL MODEL: BIA

After identifying the Basic concept as the most promising AFO design, in terms of satisfying the client and patient needs, several variables were selected to optimize the results. The following section presents the final optimization of the Basic concept, which lead to the final design of the BIA. The optimization process was divided into two phases. In Phase I, the team considered two main variables: manufacturing material and the inclination of the posterior strut with respect to the sole. The selection of materials was narrowed down to three options using a scoring matrix, after which these three materials were paired up with three inclination angles, resulting in a total of nine concepts for optimization. The final result of Phase I was a combination of a material of PC-ISO plastic and an inclination angle of 90°. In Phase II, the Basic (PC-ISO, 90°) concept was further optimized by varying the thickness of the posterior strut until the most optimal results were achieved. The thickest cross-section area of posterior strut was increased by 3 mm to a total of 7 mm. The sole was thickened from 2.5-3 mm for the final design, which provided the provided the patient with a spring-back force of 168N.

4.1 Material Selection

The 3D printer used in the project was the Fortus 400mc due to its large capacity, and the material selected to manufacture the final model was narrowed down from the 13 options that the Fortus 400mc was capable of printing, down to three: PC, PC-ISO, and PPSF. The following section details the selection of a 3D printer in Winnipeg and the scoring process used to select the top ranking materials.

4.1.1 Material Printer Selection

A number of 3D printers offered by the North Forge Fabrication Lab in Winnipeg, a facility recommended by the client at AO, were taken into consideration. The 3D printers available at North Forge considered for this project are summarized in TABLE VIII [13].

TABLE VIII
CAPACITY OF 3D PRINTERS AND MATERIALS AVAILABLE AT NORTH FORGE

3D Printer	Capacity l x w x h (mm)	Materials	Reference
Objet260 Connex	255 x 200 x 252	Engineering plastics, rubber-like materials, polypropylene	[14]
uPrint Plus	203 x 203 x 152	Thermoplastics	[15]
Ultimaker 2 Extended	223 x 223 x 305	PLA, ABS, Exotics	[16]
Fortus 400mc	406 x 355 x 406	ABSi, ABS-M30, ABS-M30i, ABS-ESD7, PC-ABS, PC-ISO, PPSF, Ultem 1010, Ultem 9085	[16] [17]
Sindoh 3Dwox	210 x 200 x 195	PLA, ABS	[18]
Zprinter 650	254 x 381 x 203	High performance composites	[19]
CubeX	275 x 265 x 240	PLA, ABS	[16]

The most important criteria used to decide which 3D printer would be used to print the final design concept was its capacity. The approximate dimensions of the AFO were expected to be 265 mm x 104 mm x 340 mm, as shown in TABLE IV, and comparing these dimensions with the capacities of 3D printers in TABLE VIII, it is clear that the only 3D printer large enough to accommodate the AFO is the Fortus 400mc. As a consequence, the brace was limited to the printing material specific to the Fortus 400mc.

4.1.2 Material Scoring

The material scoring process was used to narrow down the number of possible materials that could be used to manufacture the final design from 13 to three. This scoring process included analyzing each material, with respect to the other materials, based on six material properties: tensile strength, elongation at break, temperature distortion, elastic modulus, fracture strength, and specific gravity. Using the analysis, the priority of each material was established. The following sections describe the physical properties used to evaluate the 3D printing materials, and the scoring process.

4.1.2.1 Material Scoring Criteria

The types of material available for the Fortus 400mc were ABSplus, ABSi, ABS-M30, ABS-M30i, ABS-ESD7, ASA, Nylon 12, PC, PC-ABS, PC-ISO, PPSF, Ultem 1010 and Ultem 9085 [20]. In order to determine which material had the greatest potential for final optimization, the materials were compared based on their tensile and fracture strength, elongation percentage, elastic modulus, distortion temperature, and specific gravity. The following section provides a brief description of the importance of the properties selected.

Tensile strength (TS)

The tensile strength of a material is a measure of the ability to resist failing when subjected to tensile stress, where a higher value indicates a higher tolerance. The tensile stresses at the thinner cross-sections and near the sole of the AFO were the primary concern because these regions present the greatest stress regions, and consequently where component failure would typically occur. Therefore, materials with high tensile strength were sought. Additionally, 3D printing provides the ability to print materials along different axes depending on the tensile strength requirements of the design. Three of the 13 materials available for the Fortus 400mc have different tensile strengths along the xz and zx directions so that, when the design of the final concept has been fully optimized, the direction of printing can additionally be optimized. However, for the purpose of rendering the material scoring conservative, the lower tensile strength was used.

Elongation at break (EB)

The elongation at break is a measure of how much the AFO can distort prior to failure and how much the structure stretches with time. The latter was particularly important because the brace depends on its elasticity to provide plantarflexion support. The materials that had sufficient elongation to be capable of stretching if a large force were applied were sought, but not so much that it no longer provides sufficient support. However, for the purpose of this analysis, a higher elongation was favoured since the patient needs room to "break-in" the brace.

18

Temperature distortion (T)

At high temperatures, plastics have a tendency to relax, which would lower the overall properties of the structure. As a consequence, the brace could perform less effectively. If the temperature were high enough to plastically deform the AFO, then the brace could lose its shape entirely causing the brace to fail. Therefore, the temperature at which the AFO would distort should be larger than the maximum operating temperature in Manitoba climate.

Elastic modulus (E)

The spring-back force of the AFO is highly dependent on the elastic properties of the material used to fabricate the brace, which relies highly on the stiffness of the material. A posterior strut with a higher stiffness requires more effort to bend forwards, but also produces a greater spring-back return for that effort. The COTS AFO is relatively flexible, allowing the posterior strut to bend forwards to the sole of the brace. However, this is unnecessary because the brace is never bent at that angle when used. The objective was to 3D print the final design using a material with high stiffness, and consequently a high elastic modulus. As a result, a mid-range value was necessary during optimization.

Fracture strength (FS)

The fracture strength was primarily a concern during heel strike because a greater percentage of the weight of the patient is subjected onto the brace during this motion. In this case, a material that had a high fracture strength was sought such that the brace would be better equipped to handle these repeated high impact forces during the gait cycle.

Specific gravity (SG)

The specific gravity is the ratio of the density of the material with respect to water, such that this parameter is a measure of the weight of the AFO that can be expected for a given volume of material. The weight of the brace was one of the needs identified by the client, and should be as low as possible to help the patient achieve a natural gait cycle.

The material properties of the 3D printing materials for the Fortus 400mc are shown in TABLE IX.

TABLE IX
SUMMARY OF 3D PRINTING MATERIAL PROPERTIES FOR FORTUS 400MC

| Printing Material | Material Selection Criteria | | | | | | Reference |
	TS (MPa) xz/zx	EB (%)	T (°C)	E (MPa)	FS (MPa)	SG	
ABSplus	31/31	6	82	2200	35-55	1.04	[21]
ABSi	37/37	4.4	73	1920	62	1.08	[22]
ABS-M30	31/26	2-7	82	2180-2230	48-60	1.04	[23]
ABS-M30i	36/36	4	82	2400	61	1.04	[24]
ABS-ESD7	36/36	3	82	1900	61	1.04	[25]
ASA	29/27	3-9	91	1950-2010	48-60	1.05	[26]
Nylon 12	32/28	5.4-30	55	1138-1282	61-67	1	[27]
PC	40/30	2.5-4.8	127	1944-1958	68	1.2	[28]
PC-ABS	41/41	6	96	2400	68	1.1	[29]
PC-ISO	57/57	4	127	2000	90	1.2	[30]
PPSF	55/55	3	189	2100	110	1.28	[31]
Ultem 1010	64/42	2-3.3	213	2200-2770	77-144	1.27	[32]
Ultem 9085	47/33	2.2-5.8	153	2150-2270	68-112	1.34	[33]

4.1.2.2 MATERIAL SCORING MATRIX

The aforementioned material scoring criteria were evaluated relative to each other using a weighting matrix, where the letter shown at the intersection of the two criteria indicated that this criterion took precedence over its competitor. The total number of occurrences where a criterion succeeded over its competitor was totalled, which was then divided by the number of possible occurrences, which gave the relative weight of the criterion. The results of this matrix are shown in Figure 14.

Criteria ID.	Criteria	Tensile strength (Mpa)	Elongation at break (%)	Temperature distortion (°C)	Elastic modulus (MPa)	Fracture strength (MPa)	Specific gravity	Occurrence	Weight Percentage (%)
		A	B	C	D	E	F		
A	Tensile strength (Mpa)		A	A	D	A	A	4	27
B	Elongation at break (%)			B	D	E	F	1	7
C	Temperature distortion (°C)				D	E	C	1	7
D	Elastic modulus (MPa)					D	D	5	33
E	Fracture strength (MPa)						E	3	20
F	Specific gravity							1	7

Figure 14. Scoring matrix identifying the weight of each material scoring criteria with respect to the project.

As expected, the elastic modulus had the greatest weight while fracture and tensile strength had a slightly lower weight. The elongation at break, temperature distortion, and specific gravity were weighted the lowest because the former two would take much longer to affect the effectiveness of the brace, while the latter was a matter of convenience rather than functionality.

4.1.2.3 MATERIAL SCORING ANALYSIS

The ideal elastic modulus must be able to provide more stiffness than the COTS AFO, but not so stiff that the patient would be required to overexert themselves unnecessarily. It is for this reason that those materials with an elastic modulus less than that of the COTS design, namely Nylon 12, were eliminated along with those with an elastic modulus greater than 2200 MPa. The materials that remained were ABSi, ABS ESD7, ASA, PC, PC-ISO, and PPSF.

These six materials were then scored in comparison to one another to gage their relative performance. A good performance was indicated using a rank of "10" while the decreasing performance of the remaining materials received a correspondingly

lower rank. The product of the rank and weight of a particular material and material scoring criteria offered a score, after which all of the individual scores for a material were summed giving a total score. The final score of the material was then assigned a total rank depending on how the total score compared with the other total scores, where a high scoring material received a rank of "1", and an increased rank indicated a lower total score. The results of this analysis are shown in TABLE X.

TABLE X
SUMMARY OF MATERIAL SCORING

		Material									
		ABSi		ABS-ESD7		ASA		PC		PC-ISO		PPSF	
Criteria	Weight	Rank	Score	Rank	Score	Rank	Score	Rank	Score	Rank	Score	Rank	Score
TS	0.27	7	1.89	6	1.62	5	1.35	8	2.16	10	2.70	9	2.43
EB	0.07	8	0.56	6	0.42	10	0.70	9	0.63	7	0.49	6	0.42
T	0.07	6	0.42	7	0.49	8	0.56	9	0.63	9	0.63	10	0.70
E	0.33	6	1.98	5	1.65	9	2.97	7	2.31	8	2.64	10	3.30
FS	0.20	7	1.40	6	1.20	5	1.00	8	1.60	9	1.80	10	2.00
SG	0.07	8	0.56	10	0.70	9	0.63	7	0.49	7	0.49	6	0.42
Total Score		6.81		6.08		7.21		7.82		8.75		9.27	
Total Rank		5		6		4		3		2		1	
Continue?		N		N		N		Y		Y		Y	

As shown in TABLE X, PPSF, PC-ISO and 3D printable PC were the top ranking materials capable of providing the necessary properties for the AFO. All three of these materials were tested on the final concept selected for final optimization to determine which best satisfies the needs of the client.

4.2 INCLINATION ANGLE SELECTION

In order to optimize the forward propulsion of the AFO, it was not only important to consider various 3D printing materials but also to investigate different posterior strut neutral positions. The posterior strut was considered to be perpendicular to the sole, but the results could be improved by shifting the angle forwards or backwards. The following sections discuss the benefits and drawbacks of these two cases, and presents their respective displacement analysis.

4.2.1 POSTERIOR STRUT NEUTRAL POSITIONS

Increasing the angle between the posterior strut and the sole, the force required to move the strut from this position to the desired inclination prior to heel lift-off would be increased, but the return moment that supplies the plantarflexion support would also be increased as a result. An angle of 95°, from the sole to the posterior strut, represents the angle between the knee, heel, and toes prior to heel strike [34], as shown in Figure 15 a). On the other hand, some plantarflexion support would be lost in decreasing the angle between the posterior strut and the sole, but the force required to move the strut forward would be decreased and the dorsiflexion support during the forward swing motion of the affected foot would be improved. An angle of 85° was selected to mirror the change of five degrees, this time inclined towards the sole instead of away from it, as shown in Figure 15 c).
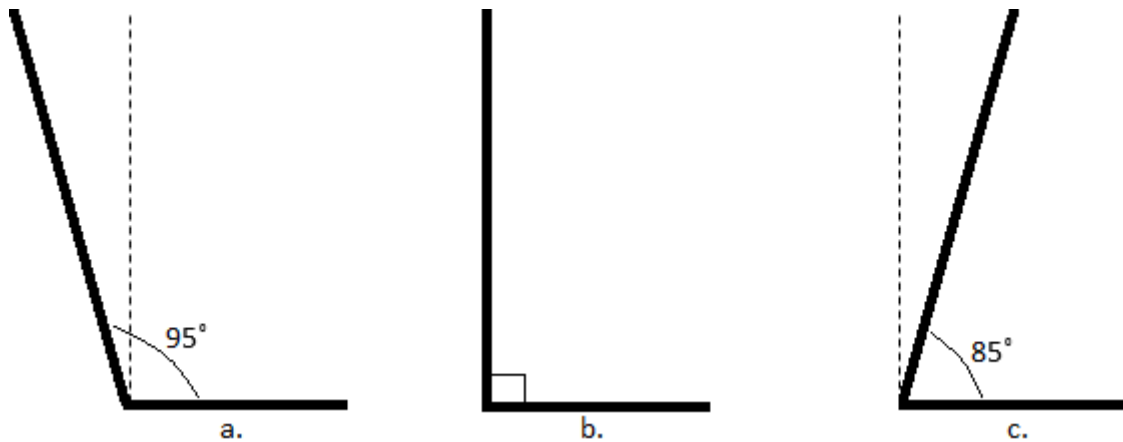
Figure 15. AFO with an inclination angle of a) 95°, b) 90°, and c) 85°, between the posterior strut and the sole.

During this optimization, the primary concern was to verify how a change in posterior strut angle influences the forward propulsion of the AFO, and whether this change outweighed the drawbacks.

4.2.2 POSTERIOR STRUT DISPLACEMENTS

During concept selection in Section 3.1.1.1, it was assumed that the posterior strut was a linear elastic beam in bending where the force applied to the AFO was directly proportional to the distance that the brace displaces. However, the forces calculated

23

during concept selection was on a simplified shape merely to gage an idea of how the different concepts reacted to applied loads. Moving forwards, the analysis was more complex: the forces required to displace the AFO were solved for numerically using FEA. The displacements required for the 95°, 90°, and 85° strut neutral positions are shown in Figure 16.
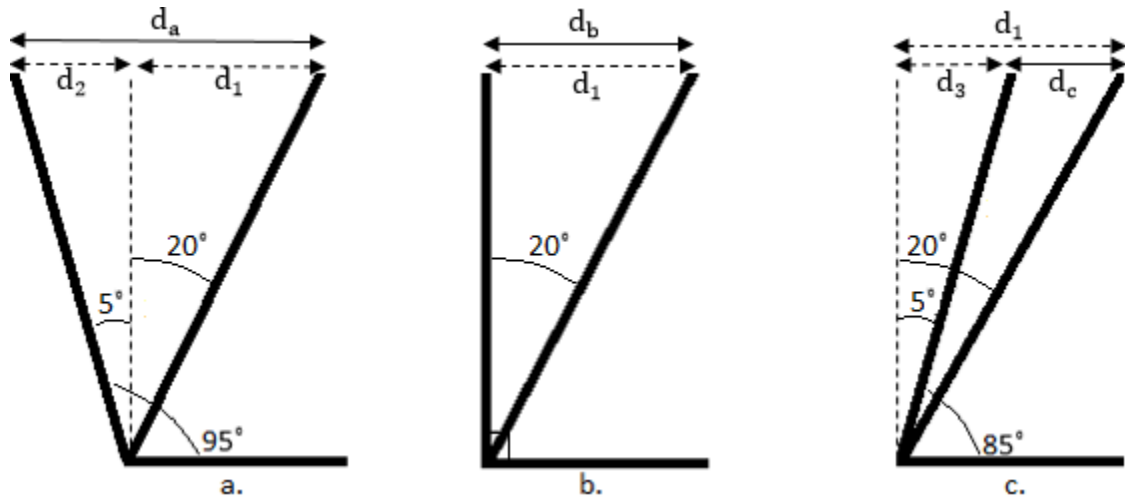
Figure 16. Schematic of the displacement of an AFO at different inclinations where the posterior strut is a) 95°, b) 90°, and c) 85° away from sole.

The displacements in Figure 16 were calculated by adding or subtracting the displacement that stems from the starting position of the posterior strut, which was the common displacement. The displacement of an initial posterior strut angle of 95° was calculated using equation (5).

$$d_a = L \tan \theta_1 + L \tan \theta_2 \tag{5}$$

The displacement of an initial posterior strut angle of 90° was calculated using equation (4) on page 7, while that of the displacement of an initial posterior strut angle of 85° was calculated using equation (6).

$$d_a = L \tan \theta_1 + L \tan \theta_2 \tag{6}$$

TABLE XI summarizes the results of equations (4), (5), and (6).

24

TABLE XI
EQUATIONS REQUIRED TO CALCULATE DISPLACEMENT OF AFO MODEL FOR
VARIOUS POSTERIOR STRUT INITIAL POSITIONS

Material	Equation Number	Equation	Angles (degrees)	Displacement (m)
All	(4)	$d = \tan\theta$	90	0.124
	(5)	$d_a = L\tan\theta_1 + L\tan\theta_2$	95	0.153
	(6)	$d_a = L\tan\theta_1 + L\tan\theta_2$	85	0.094

4.3 OPTIMIZATION

After the three possible materials and the three possible inclinations of the posterior strut were identified, there were nine concepts to optimize as part of the first optimization phase. For ease of reference, these concepts were named the Basic (PC, 95°), Basic (PC, 90°), Basic (PC, 85°), Basic (PC-ISO, 95°), Basic (PC-ISO, 95°), Basic (PC-ISO, 95°), Basic (PPSF, 95°), Basic (PPSF, 95°) and Basic (PPSF, 95°) concepts. The following sections take a look at the displacements of these possibilities, the numerical approach to determine the applied forces, and the FEA to determine the optimal combination.

4.3.1 FORCE EXERTED BY LEG

Up to this point in the project, more focus was directed towards how much force was required to displace the AFO a prescribed distance, and less on how much spring-back force the brace could produce. In order to determine a reasonable value of force applied to the brace in order to displace it, the amount of force that a normal leg could exert on the ground prior to heel lift-off was considered. The following sections consider both the static and dynamic motions present during the gait cycle stance prior to heel lift-off of the affected foot.

4.3.1.1 STATIC ANALYSIS

In order to simplify the calculations, the affected leg was considered to be a uniform, rigid beam rotation about a pivot point because, during the swing phase of the non-affected foot, the body appears to be pivoting about the heel of the affected foot

until its maximum displacement is reached. A depiction of the static position of a person prior to heel lift-off of the affected foot is shown in Figure 17.
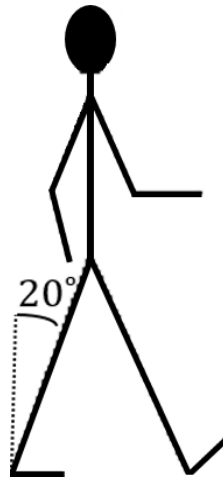
Figure 17. Depiction of a person whose affected foot has bend forwards to its maximum position prior to heel lift-off.

In order to gain an understanding of where forces were acting on the body, the critical proportions of a person were identified. Then, the affected leg was isolated to analyze the static mass distribution acting on the affected leg. It was found that the majority of the mass of the person was exerted at the extremity of this beam, away from the pivot point, and a smaller portion of the total was exerted at the center of mass of the leg, as shown in Figure 18.
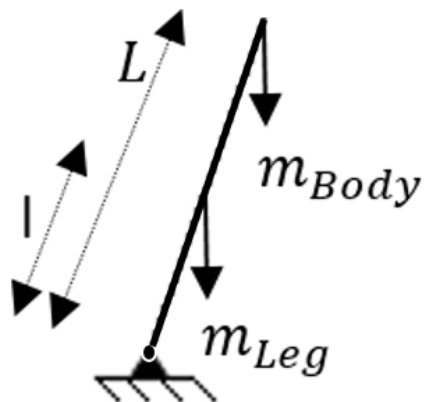
Figure 18. Mass distribution of the affected foot prior to heel lift-off as well as the distances of these masses from the pivot point at the heel of the affected foot.

Proportions of the Affected Leg

The average length of a leg is approximately 45% of the height of the individual, such that the leg length can be approximated using equation (7), where H represents the height of the individual [35].

$$L = 0.45H \qquad (7)$$

The distance from the pivot point at the heel to the center of mass of the leg is a fraction of the leg length, found using equation (8), where the length of the leg is taken from the foot to the greater trochanter [36].

$$l = \frac{4L}{9} \qquad (8)$$

Mass Distribution

The stance where the non-affected foot is in contact with the ground was under consideration and so the mass of the body exerted on the one leg was less than that of the total mass of a person, found using equation (9).

$$m_{body} = m - 2m_{leg} \qquad (9)$$

The mass of a leg is similarly a fraction of the total mass of a person, found using equation (10), where m is the total mass of this person [36].

$$m_{leg} = \frac{m}{7} \qquad (10)$$

Height and Mass on an Average Male Adult

The parameters, shown in Figure 18, come from two bodily parameters: the height and weight of the person. In the case of the project, the AFO was designed for a specific male, adult patient. Therefore, the height and weight used in this analysis were taken as those of an average male adult, and are summarized in TABLE XII.

TABLE XII
DIMENSIONS OF AN AVERAGE MALE ADULT

Dimension Description	Reference	Dimension Value
Height	[37]	1.77 m
Total Mass	[9]	86.18 kg

4.3.1.2 Dynamic Analysis

At this point, it was important to find the center of mass of the entire rotating beam as well as the location of this center of mass to simplify the structure, which were found using equation (11) and (12), respectively [38].

$$m_r = \sum m_i r_i = m_{leg}l + m_{body}L \tag{11}$$

$$r = \frac{\sum m_i r_i}{M} = \frac{m_{leg}l + m_{body}L}{m_{leg} + m_{body}} \tag{12}$$

Now, considering the leg to be the rotation beam shown in Figure 19, there were two accelerations acting on the beam aside from gravity: the tangential (a_t) and normal (a_n) acceleration.
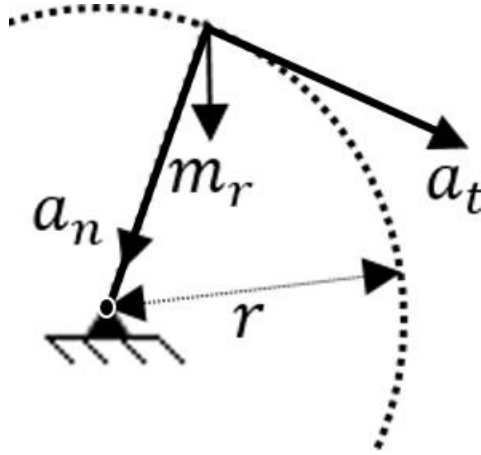
Figure 19. Polar coordinate accelerations exerted on a rotating beam, representing the affected leg.

The leg was assumed to be moving at a constant velocity. As a result, the tangential acceleration was zero and the normal acceleration was calculated using equation (13) [39], where v represented the gait cycle velocity that averaged around 1.33 m/s (80 m/min) [40].

$$a_n = \frac{v^2}{r} \tag{13}$$

The resulting accelerations that were exerted at the extremity of the beam are shown in Figure 20.
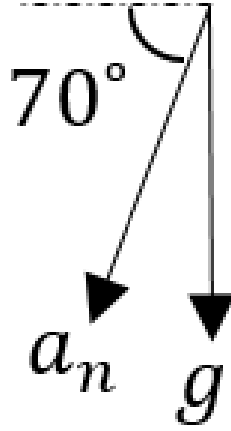
Figure 20. Reacting accelerations of the rotation beam.

The total acceleration was found using equation (14), and x and y components of the accelerations in Figure 20.

$$a = \sqrt{a_x{}^2 + a_y{}^2} \qquad (14)$$

The final force exerted by the leg was then calculated using equation

$$F = m_r a \qquad (15)$$

4.3.1.3 RESULTS OF STATIC AND DYNAMIC ANALYSIS

The results of the static and dynamic analysis from Sections 0 and 4.3.1.2, respectively, are summarized in TABLE XIII.

TABLE XIII
EQUATIONS REQUIRED TO CALCULATE THE FORCE APPLIED EXERTED BY A LEG
AND THE CORRESPONDING RESULTS OF EACH EQUATION

Equation Number	Equation	Result
(7)	$L = 0.45H$	0.80 m
(8)	$l = \dfrac{4L}{9}$	0.35 m
(9)	$m_{body} = m - 2m_{leg}$	12.31 kg
(10)	$m_{leg} = \dfrac{m}{7}$	61.54 kg
(11)	$m_r = \sum m_i r_i = m_{leg}l + m_{body}L$	53.42 kg
(12)	$r = \dfrac{\sum m_i r_i}{M} = \dfrac{m_{leg}l + m_{body}L}{m_{leg} + m_{body}}$	0.62 kg
(13)	$a_n = \dfrac{v^2}{r}$	2.87 m/s²
(14)	$a = \sqrt{a_x{}^2 + a_y{}^2}$	12.50 m/s²
(15)	$F = m_r a$	667.75 N

As shown in TABLE XIII, the force that an average male adult can exert prior to heel lift-off of the affected foot is 667.75 N. However, it is important to note that this was an approximation that was largely constrained by the following factors:

i) Designed for a male of average height and weight, and approximate limb lengths

ii) Did not take into consideration the bending of the leg at the knee

iii) Assumed a constant gait cycle velocity

As previously mentioned, the forces required to displace the AFO the desired distance will be solved for numerically using FEA in the following sections, but this

analysis provided a reference for comparison to gage whether the stiffness of the brace is in the appropriate range.

4.3.2 Phase I Optimization

The following sections highlight the optimization of the Basic model when considering the shape of the patient's leg posterior strut and sole. Additionally, the Basic model was modeled at three different inclination angles for further optimization. FEA tests were conducted to determine how each of the models reacted to the prescribed displacement, where the areas of high stress formed, the degree of optimization required to achieve a safety factor (SF) of 2, and the greatest amount of forward propulsion. Lastly, this section outlines the methodology of how the final material and inclination angle were selected, and summarizes the results of the ideal combination selected.

4.3.2.1 Remodelling the Basic Concept

As mentioned in Section 4.2, the Basic design was analyzed at three different inclinations angles to determine which is most suitable to provide the greatest amount of forward propulsion. The four models considered in Section 3.1 were modeled based on the dimensions of the COTS AFO and a generic model of a calf [16]. However, since the final design is to be tested on a patient, the team customized the shape of the brace to the patient. In order to accomplish this task, the team met with a patient from AO and received a 3D scan of the patient's leg from the client. Figure 21 shows the 3D scan that was provided.

Figure 21. 3D scan of the leg of one of patients from AO suffering from plantarflexion and dorsiflexion weakness, using Canfit™ P&O modifying CAD software.

From the 3D scan, the Basic concept was remodeled to accommodate both the location of the patient's ankle bone and the fibular head. The height of the brace was left as 340 mm to ensure the patient's fibular head would not be irritated. The dimensions of the sole and the calf were adjusted from the preliminary Basic model, so that the brace would form to the shape of the patient's leg and be able to slip into the patient's shoe. Figure 22 illustrates the newly dimensioned Basic model at the three inclinations angles that were further analyzed.

a)   b)   c)
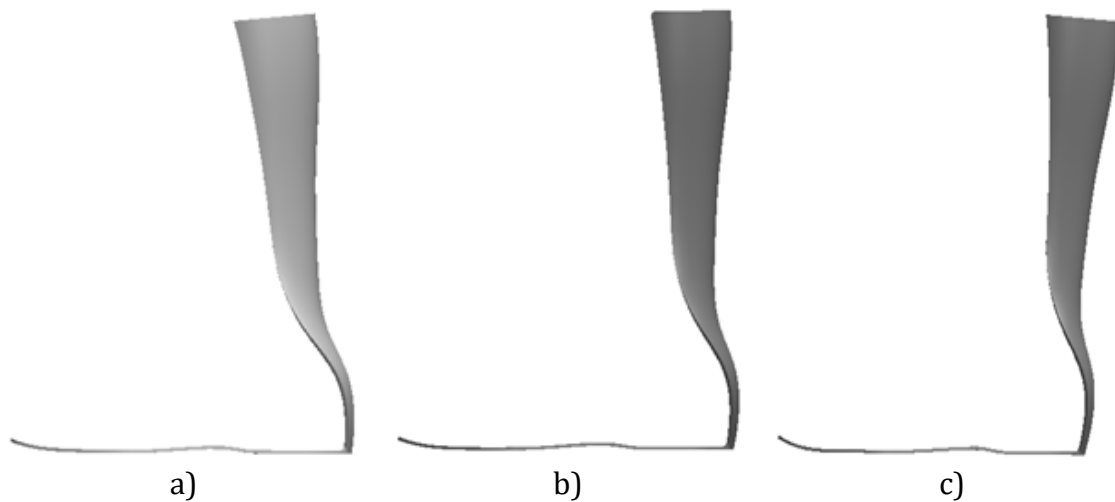
Figure 22. Models of the Basic concept dimensioned to the patients affected leg at an inclination of a) 85°, b) 90°, and c) 95°.

The sole of the Basic model was also modified to suit the needs of the patient. When comparing Figure 4 on page 2 to Figure 22, it can be seen that the arch along the sole is greatly decreased in Figure 22. This decrease is due to the fact that the patient wears an insole on top of the AFO for extra support and comfort. Therefore, the complexity of the arch in Figure 4 on page 2 was removed. From here, the three models were analyzed with the three materials selected in Section 4.1.2.3 each with the appropriate applied displacements.

4.3.2.2 FEA of Phase I Optimization

Similar, to the FEA performed in Section 3.1.1.2, the objective of this first analysis was to determine which concept was best suited to meet the needs of the client. More specifically, the objective of this analysis was to determine which combination of material and inclination angle will provide the greatest amount of spring-back force when reaching the desired forward displacement while achieving a SF of 2. Additionally, the design could not be so bulky as to become uncomfortable for the patient. The FEA results were compared to one another by considering the amount of force required to displace the AFO and the high stress values along the posterior strut. This type of comparison was used instead of the visual stress distribution inspection, performed previously analyzed in Section 3.1.1.3, to reduce the subjectivity, and render the analysis quantitative.

To analyze each of the three models using the three different materials, the material properties in TABLE IX on page 20 were inputted into SolidWorks®. It was important to note that PC has two different tensile strengths depending on the direction the material is printed. Since only one set of tensile strengths and elastic moduli could be used for the material property input in SolidWorks®, the higher tensile strength and lower elastic modulus was selected, in order to provide a desired amount of stretch to spring-back force for maximum propulsion. This set of properties for PC was the xz direction, with a tensile strength of 40 MPa and an elastic modulus of 1944 MPa. Once all of the material properties were inputted into SolidWorks®, the following FEA setup was followed for each of the nine combinations.

Fixture

To simulate the heel of the brace popping up from the ground as the leg reaches a maximum of 20 degrees, the fixture along the bottom of the sole was modified from the previous fixture in the preliminary FEA in Section 3.1.1.2. The fixture was separated into two sections where 2/3 of the sole was fixed to the sole of a shoe while the other 1/3 of the sole was set up as a slider fixture, as shown in Figure 23.
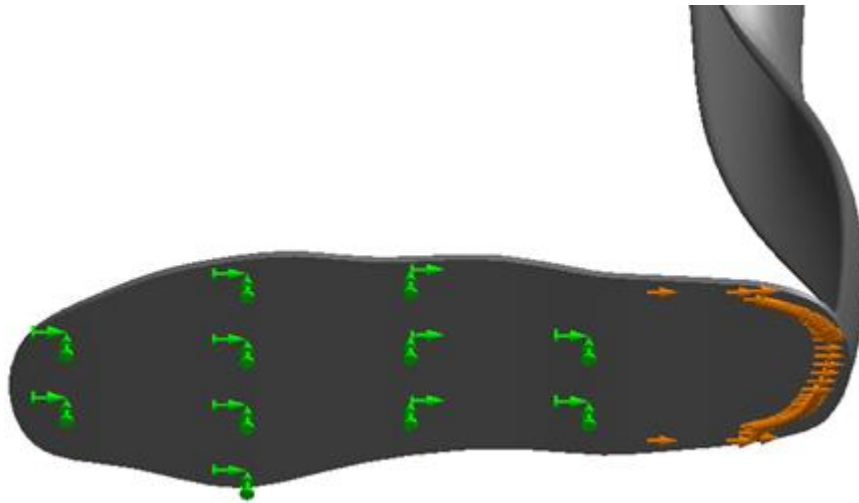
Figure 23. Phase I FEA fixture set up along the sole of the AFO with 2/3 of the sole fixed to the sole of a shoe and 1/3 of the sole left as a slider fixture.

The fixed portion of the sole is highlighted with green arrows, which prevented the AFO from moving up off the ground as the posterior strut is displaced. The slider portion of the sole, highlighted in orange arrows, simulated the sole of the AFO sliding along the sole of a shoe and pulling up as the posterior strut is pushed forward with each step.

Prescribed displacement

To simulate the AFO moving 20° forward while staying attached to the patient's leg, a prescribed displacement was set as the second boundary condition in SolidWorks®. This feature allows the required distance and direction of motion to be inputted along the specified area of the AFO which must be displaced. Figure 24 illustrates this boundary condition.
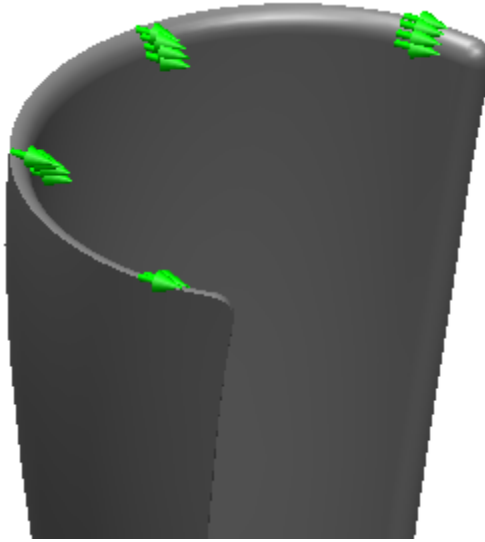
Figure 24. Direction and location of prescribed displacement applied to the AFO during FEA setup.

The green arrows, shown in Figure 24, were set to point away from the posterior strut, simulating the motion of the leg moving towards the toes when walking. The arrows were placed along the top of the posterior strut to simulate the AFO displacing linearly as it would while attached to the patient's leg. Although the Velcro strap around the AFO covered a greater surface area than what is shown in Figure 24, the method of applying the load in this analysis was energetically equivalent. Lastly, the distance that the top surface must be displaced was set with respect to which inclination angle was analyzed.

Curvature-based mesh
The final boundary condition set in FEA was the mesh size on each model. As each model has a different material and inclination angle, the mesh was unique to each model. A curvature based mesh was applied to each model to accommodate the complex curves and fillets, and to ensure the curves were thoroughly analyzed. Since the results of the FEA would be compared by the value of high stress in the model, it was important to ensure the results from the FEA were reliable. FEA is considered reliable if the stress converges to one value after multiple iterations of FEA with a decreasing mesh size. As the mesh size decreased, the amount of

tetrahedral elements analyzed increased. Therefore, the smaller the mesh the more accurate the FEA becomes. Figure 25 illustrates the first mesh applied to the Basic (PC-ISO, 90°) model and the decreased mesh size where that the models FEA results converged.

a)   b)
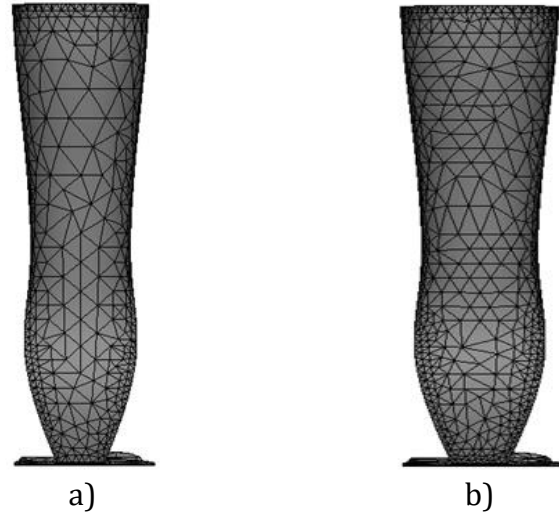
Figure 25. Curved-based mesh applied to the Basic (PC-ISO, 90°) model with a mesh size of a) 21.0 mm and b) 16.5 mm.

For each iteration from 21 mm to 16.5 mm, the stress and the number of tetrahedral elements were recorded. The stress was recorded at the area of highest stress and at the same coordinate on the AFO to remove any uncertainties in the reliability of the FEA results. The results of the stress and the respective number of elements were plotted in a convergence plot to show the reliability of the Basic (PC-ISO, 90°) model, as shown in Figure 26.
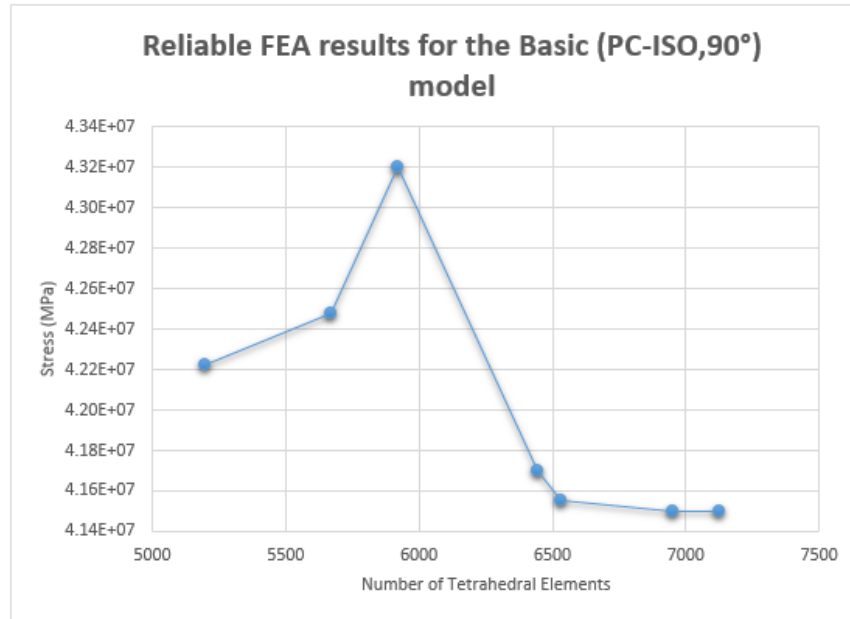
Figure 26. Convergence plot for the Basic (PC-ISO, 90°) model for a mesh size decrease from 21 mm to 16.5 mm.

The stresses converged after reducing the mesh size seven times, as shown in Figure 26, as the blue line stabilizes (i.e. plateaus) at the maximum number of tetrahedrals: 7150. The stress and number of tetrahedral elements were recorded for each of the nine combinations and convergence plots were developed to confirm the results of the FEA. The convergence plots for the remaining eight models can be found in Appendix B.

FEA results

The results of each model with a front and side view is shown in Figure 27 through Figure 29, highlighting the high and low stresses in each model with a colored stress scale respective to each material's ultimate strength with a SF of two applied.
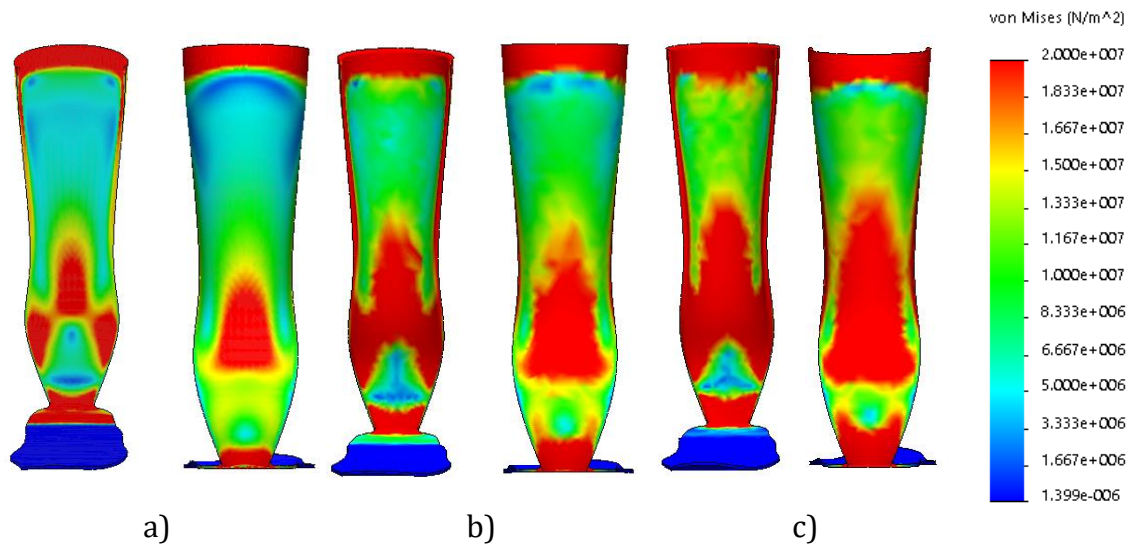
Figure 27. Stress distribution in the Basic models with respect to the SF of 2 stress scale for PC at a prescribed displacement of a) 85°, b) 90°, and c) 95°.

As the angle between the sole of the AFO and the posterior strut increased, the stress in the models shown in Figure 27, also increased along the front and back surfaces of the posterior strut.
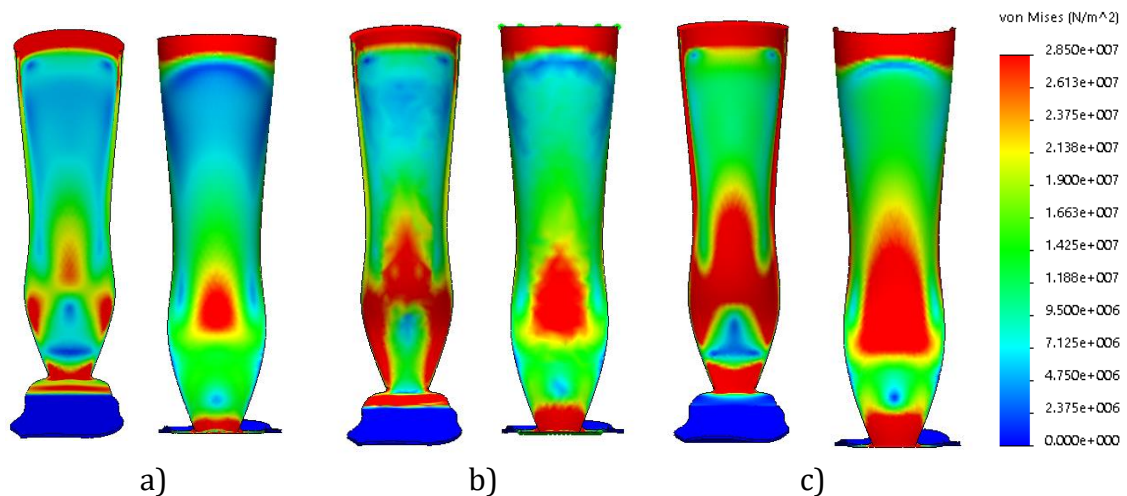
Figure 28. Stress distribution in the Basic models with respect to the SF of 2 stress scale for PC-ISO at a prescribed displacement of a) 85°, b) 90°, and c) 95°.

A linear increase in stress was noticed between PC-ISO 85° and PC-ISO 95°, as shown in Figure 28.
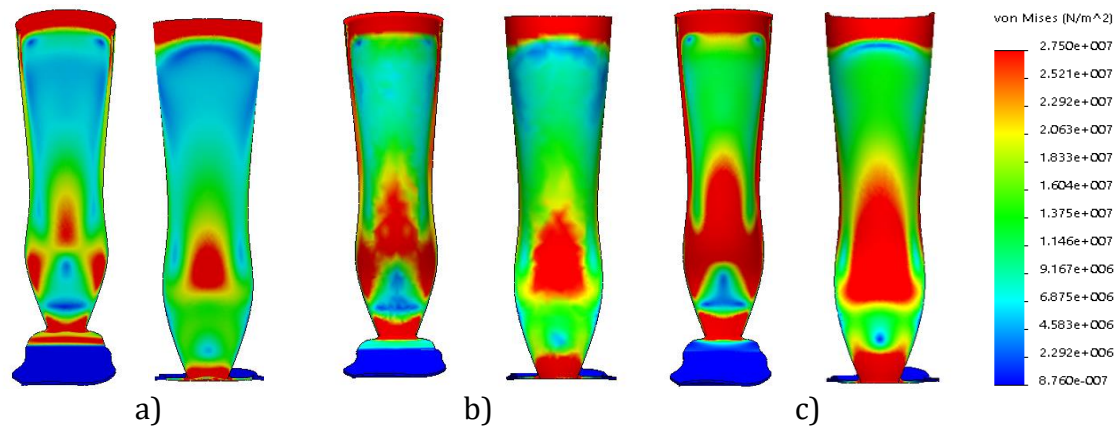
Figure 29.Stress distribution in the Basic models with respect to the SF of 2 stress scale for PPSF at a prescribed displacement of a) 85°, b) 90°, and c) 95°.

Similar to the pattern of stress distribution, shown in Figure 27, there was an increase in stress along the front and back of the posterior strut as the angle increases for the three models shown in Figure 29.

Since each set of material displayed a similar relationship between the increase in the inclination angle and stress concentrations, a more thorough numerical comparison was made to determine which of the nine combinations was capable of providing the greatest amount of spring-back force. For comparison, the stress on each model along the back of the posterior strut was measured to ensure consistency between models, so that the change in stress would be comparable. The amount of required force to displace each model to their respective displacement and weight were recorded, and if the FEA models provided a reliable result by converging was also documented. TABLE XIV summarizes all of the required values from the nine combinations for a numerical comparison.

TABLE XIV
RESULTS OF THE BENDING STRESS, SPRING-BACK FORCE, WEIGHT,
CONVERGENCE AND TENSILE STRENGTH OF THE NINE BASIC MODEL
COMBINATIONS IN SOLIDWORKS FEA

Material and Angle	Bending Stress (MPa)	Spring-Back Force (N)	Weight of AFO (g)	Tensile Strength (MPa)	Convergence
(PC, 85)	28.80	221.62	246.86	40	Y
(PC, 90)	37.94	363.00	246.63	40	Y
(PC, 95)	49.00	561.00	245.85	40	Y
(PC-ISO, 85)	30.77	238.90	246.86	57	Y
(PC-ISO, 90)	38.87	374.02	246.63	57	Y
(PC-ISO, 95)	55.60	577.80	245.85	57	Y
(PPSF, 85)	31.99	247.93	263.30	55	Y
(PPSF, 90)	41.16	391.57	263.16	55	N
(PPSF, 95)	58.82	606.46	262.24	55	Y

To analyze the results of the FEA performed, the needs of the client had to be considered, and the final result of the comparison needed to reflect the main needs of the client. The number one need provided by the client was that the AFO must be able to provide the greatest amount of forward propulsion during the gait cycle, which is directly related to the spring-back force in TABLE XIV. Additionally, it is required that the brace not fail by fracturing as the individual uses the AFO, which is the relationship between the bending stress and the tensile strength. A need provided by the patient was that the brace not be too bulky, which is directly related to the spring back force and how close the bending stress is to the SF, and the weight of the AFO. To compare how close the bending stress of each design was to a SF of 2, the difference between the bending stress and the tensile stress was calculated for each model, TABLE XV summarizes these values.

TABLE XV
DIFFERENCE BETWEEN THE BENDING STRESS AND TENSILE STRENGTH OF
EACH OF THE NINE BASIC MODEL COMBINATIONS

Material and Angle	Difference between bending and tensile strength (MPa)	Predicted spring-back force at a SF of 2 (N)
(PC, 85)	11.20	153.00
(PC, 90)	2.06	191.00
(PC, 95)	-9.00	229.00
(PC-ISO, 85)	26.23	221.27
(PC-ISO, 90)	18.13	274.30
(PC-ISO, 95)	1.40	296.80
(PPSF, 85)	23.01	213.12
(PPSF, 90)	13.84	293.04
(PPSF, 95)	-3.82	283.52

If the difference between the bending stress and tensile strength is negative, then the bending stress from the FEA results was greater than the tensile strength and if the difference was positive it meant that the bending stress along the posterior strut was already below the tensile strength. Although it seems easy to immediately eliminate the models that have a negative difference, a SF of 2 needed to be taken into consideration since the most ideal model would need to be optimized to that SF. Therefore, the predicted spring-back force at a SF of 2 was also calculated. This calculation was performed by taking the percentage of the bending stress with respect to the tensile strength, the percentage result was then applied to the spring-back force. This relationship is applicable to each model as there is a linear relationship between the tensile strength and the spring-back force. Therefore, if the bending stress were to decrease to a SF of 2 then the spring-back force would have to decrease by the same amount. The predicted values are summarized in the last line of TABLE XV.

The differences in stress and the predicted spring-back forces of each model were then compared to one another. Immediately the Basic (PPSF, 90°) model was eliminated as the FEA results did not converge, providing unreliable results for optimization. The Basic (PC, 85°) model was also immediately eliminated since the spring-back force was the lowest out of all of the models.

From there the trade-off between how thick the posterior strut would need to become to meet the SF of 2 and the decrease in spring-back force was considered. The Basic (PC, 95°) model was eliminated as the model had a low spring back force compared to the remainder of the models and the negative difference meant that the thickness of the posterior strut where the high stresses were located would need to become significantly thicker making the model too bulky. With this same methodology the Basic (PPSF, 95°) model was also eliminated due to the fact that the thickness would also have to be extremely thick to meet the SF, even though the spring-back force is significantly higher compared to other models the extreme thickness of the model would not be comfortable for the patient.

Following that elimination, the Basic (PC, 90°) model was eliminated as the spring-back force was the next lowest and the lower positive difference between bending and tensile strength meant that the thickness along the posterior strut would need to be increased significantly. The second greatest difference between tensile and bending strength was the Basic (PPSF, 85°) model, this model was compared to the Basic (PC-ISO, 85°) model with the greatest positive difference. The Basic (PPSF, 85°) model was eliminated out of the two due to the fact that the both the SF difference and the spring-back force were lower than those of the PC-ISO model, therefore giving the PPSF 85° no advantage over the PC-ISO 85° model.

The top three models ended up being the PC-ISO models. To narrow down the three models to the final model, the discrepancies between the values of SF differences and the spring-back forces of each model were compared to the other models. Firstly, the 95° model was compared to the 90° model. The difference in the SF between the two models was a significantly large separation compared to the difference between the spring-back force, meaning that the PC-ISO 95° model would need to become extremely thick along the posterior strut to accommodate a spring-back force not much higher than that provided by the 90° model, which could be a significantly thinner model. Therefore, the PC-ISO 95° model was eliminated. Lastly the difference between the PC-ISO 90° and PC-ISO 85° was analyzed. The difference between the spring-back force is greater compared to the difference between the SF

difference, therefore the greater amount of spring-back force provided by the 90°
outweighs the increase in thickness that would have to occur to the 90° model. With
these results the PC-ISO 85° was eliminated and the PC-ISO 90° model was selected
as the most optimal design of Phase I.

From here the PC-ISO 90° model was optimized further by considering the outcome
of different posterior strut inclination angles and sole thicknesses. The following
section outlines the optimization procedure that was followed.

4.3.3 Phase II Optimization

After the first phase of optimization, Phase II was implemented to further optimize
the top ranked model from Phase I, the Basic (PC-ISO, 90) model. In order to further
optimize the model, high stress regions around the base of the posterior strut were
reduced and the thickness of the posterior strut was increased until the model
satisfied a SF of 2. In order to optimize the Basic (PC-ISO, 90°) model, geometric
optimizations were performed. The following sections outline the geometric
constraints and optimizations that were considered for the final model.

4.3.3.1 Geometric constraints

In Phase I, 2/3 of the sole was fixed, while the remaining third of the sole simulated
a slider fixture when modelling the design in the SolidWorks® FEA simulation, as
shown in Figure 23 on page 34. These boundary conditions resulted in high stress
distributions in the region of the heel, as shown in Figure 30.
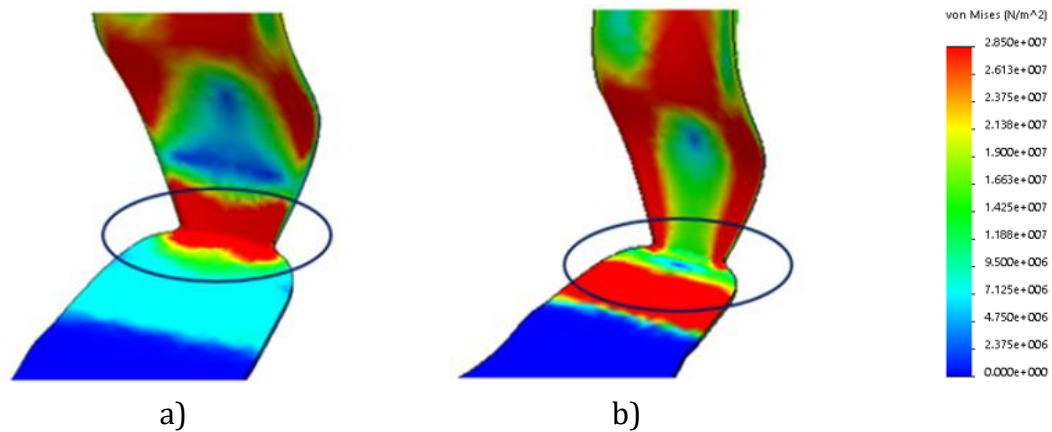
Figure 30. Stress distribution in the heel region of the Basic (PC-ISO, 90°) model
a) Over-constrained sole where 2/3 was fixed and 1/3 was fixed using a slider
b) Fully constrained sole where 2/3 was fixed and 1/3 was free

The over-constrained sole, shown in Figure 30 a), resulted in a concentration of high stresses around the heel region, while the fully constrained sole, shown in Figure 30 b), produced a greater distribution of the high stresses near the heel. The distribution of high stresses around the heel region, decreased the concentration of stresses at the heel. As a result, the boundary conditions for the sole were reanalyzed by fixing 2/3 of the sole and having the remaining 1/3 of the sole be free.

4.3.3.2 Posterior strut and sole optimization

In addition to high stress concentrations near the heel region, FEA results of the Basic (PC-ISO, 90°) model also resulted in high stresses at the back of the posterior strut, as shown in Figure 31.
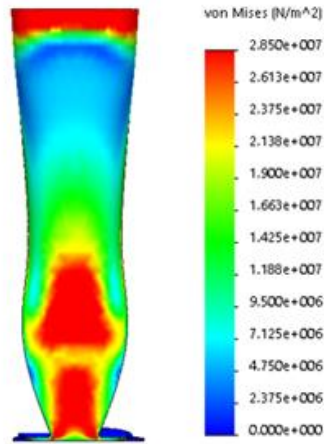
Figure 31. Stress distribution of the posterior strut with a SF of 2.

In order to reduce the stresses, shown in Figure 31, the thickness of the posterior strut was increased in these areas of high stress, as shown in Figure 32.

(a)   (b)
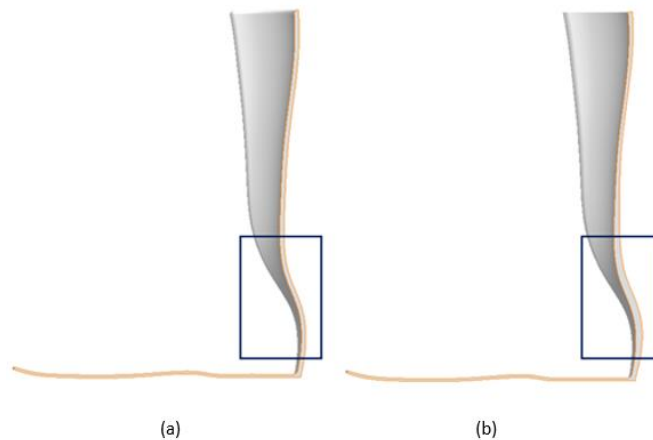
Figure 32. Cross-sectional side view of the Basic (PC-ISO, 90°) model with posterior strut thickness of a) 4.0 mm and b) 6.5 mm.

The original posterior strut thickness of the Basic (PC-ISO, 90°) model, as shown in Figure 32 a), was 4.0 mm, and Figure 32 b) illustrates the increase in the thickness of the posterior strut to 6.5mm for the Basic (PC-ISO, 90°) model. Once the thickness of the posterior strut was increased, SolidWorks® was unable to run a curvature-based mesh and resulted in a computational error. In order to correct the error, the FEA model was simplified by removing fillet along the top of the posterior strut of the model, shown in Figure 33.

45

Figure 33. Cross section at the top of the posterior strut where fillet was removed.

Once the fillets at the top of the posterior strut were removed, as shown in Figure 33, the FEA simulation was able to run the program. The FEA results showed a significant decrease in the stress distribution at the front and rear side of the posterior strut, as shown in Figure 34.
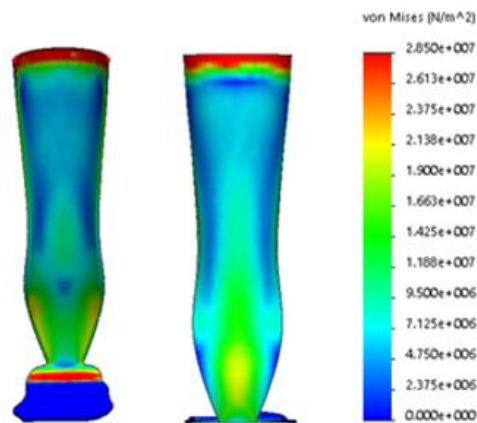
Figure 34. Front and rear view of the stress distributions in the posterior strut of the model with the removal of the fillet for a SF of 2.

The reduced stress distribution at the front and rear side of the posterior strut of the Basic (PC-ISO, 90°) model after the removal of the fillet, as shown in Figure 34, was unexpected. Theoretically, the addition of fillets at the top of the posterior strut would reduce the stress in that region, but since the addition of the fillet resulted in a higher stress distribution, the limitations of using SolidWorks® for a non-static model was confirmed. Therefore, the remainder of the analyses were performed on the model with the fillet removed, in order to obtain a more accurate representation

of the stresses in the model. The sharp edges were removed around the sides of the sole by applying the fillets, as shown in Figure 35.
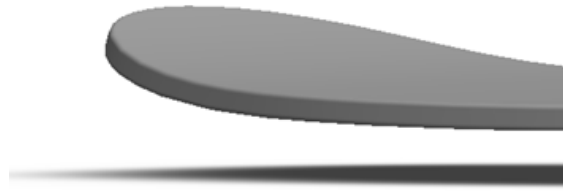
Figure 35. Fillets applied around the edges of the sole of the model.

The sharp edges of the sole were removed, shown in Figure 35, for the ease of the patient to slide the brace into the shoe and prevent discomfort.

shows the stress results from FEA as the posterior strut and sole thicknesses were increased to help eliminate the high stress areas.

TABLE XVI shows the stress results from FEA as the posterior strut and sole thicknesses were increased to help eliminate the high stress areas.

TABLE XVI
RELATIONSHIP BETWEEN THE STRESSES AND THICKNESS OF THE POSTERIOR STRUT AND SOLE
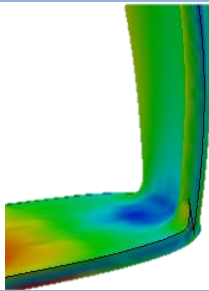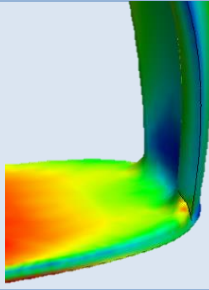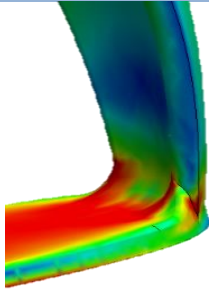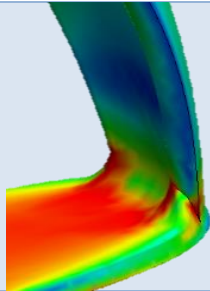
Posterior Strut		Sole		Joint	
Thickness (mm)	Stress (MPa)	Thickness (mm)	Stress (MPa)	Fillet (mm)	Redistributed Stress (MPa)
3	20.83	2.5	33.39	4	None
3	18.56	3	32.30	4	28.18
3	15.04	4	29.35	7	32.95
2.5	15.24	4	30.15	7	36.83
3	13.21	4.5	38.50	7	39.10
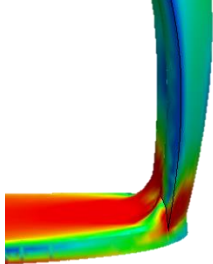
As the sole thickness increased, the stress decreased, up to thickness of 4mm, however the stress increased again once the thickness of the sole was increased to 4.5. Although it appears that when the sole thickness is 4mm, the design would be optimal; however, when the thickness of the sole was increased to 4 mm, redistributed stresses developed at the heel cap. Increasing the fillet size at the joint also did not help in reducing the high stresses.

TABLE XVII shows a visual representation of the FEA results tabulated in shows the stress results from FEA as the posterior strut and sole thicknesses were increased to help eliminate the high stress areas.

TABLE XVI. For each model, a SF of 2 was applied to the ultimate strength gradient scale.

TABLE XVII
STRESS DISTRIBUTION RESULTS AT THE JOINT OF POSTERIOR STRUT AND SOLE

Thickness (mm)		FEA Model	Observation
Posterior Strut	Sole		
3	2.5		Minimal stress distribution at the joint
3	3		Increase in stress distribution at the corners of the joint
3	4		High stress distribution at the sole, inner joint and the corner of the joint
2.5	4		Greater increase in stress distribution at the inner joint and the corner of the joint.

3	4.5		Significant increase in high stress distribution at the sole, at the joint, and at the back of joint.

The stress distribution was summarized in TABLE XVII for different posterior strut and sole thickness. It was observed that the stress distribution increases at the heel cap and the sole as the posterior strut and the sole thickness increases. A minimal stress can be observed at the heel cap with the posterior strut thickness of 3 mm and the sole thickness of 2.5 mm. Also, a high stress distribution at the heel cap and sole can be observed with the posterior strut thickness of 3 mm and the sole thickness of 4.5 mm. This result allowed the team to optimize the posterior strut thickness and sole thickness of the Basic (PC-ISO, 90°) model.

4.3.3.3 Safety Factor (SF)

The increase in the redistributed stresses occurred due to the increase in sole thickness because the joint became too stiff as the thickness increased. The strength of the material was the limiting factor here, preventing the posterior strut to bend easily and it does not overcome the stress distribution when the material thickness was increased.

The SF constraint applied to the preliminary final model were reconsidered as the design was determined to be over constrained for the applications required. This was determined as the team observed the motion of the patient's leg during the gait cycle. The initial assumption was that the maximum displacement of the leg during the gait cycle is 20 degrees. However, after assessing the patient's gait cycle, it was determined this 20° angle would be very difficult to achieve as the knee bends during the gait cycle and the 20° angle would only be achieved with a straight knee during stretching of the calf or when an individual's gait cycle is made up of long strides. Two scenarios which are difficult for an individual with plantarflexion and dorsiflexion to achieve. Therefore, the 20° angle was concluded to be the worst case

scenario for the AFO, and also the displacement that would be achieved the least often. Therefore, having a SF of 2 at the 20° position would be over constraining the design as the stiffness of the AFO flexing through the angles leading up to 20° would be too stiff and therefore, would induce high stresses and in turn increasing the possibility of fracture. With this in mind the maximum displacement of 20° still needed to be considered for the possibility of the patient using the brace while stretching. Therefore, the SF was decreased to 1.5 at an angle of 20° so that the model could be easily bend forward as it is intended to when the patient walks with it and also avoid failure by fracture at the maximum displacement.

The results of the initial FEA comparison of the nine models would result in the Basic (PC-ISO, 90°) whether a fillet was applied or not because the stresses were all linear at the back of the posterior strut during the FEA simulation. If the FEA was performed with SF of 1.5 and no fillet, the FEA results of the nine compared models would be similar. However, to a lesser degree, the Basic (PC-ISO, 90°) would be chosen as the best preliminary final design. Figure 36 shows the stress distributions at the back and the front of the posterior strut with a SF of 1.5. The results of the initial FEA comparison of the nine models still would result in the Basic (PC-ISO, 90°) whether a fillet was applied or not because the stresses were all linear. If the FEA was performed with SF of 1.5 and no fillet, the FEA results of the nine comparison models would have been similar, however to a lesser degree, the Basic (PC-ISO, 90°) still would have been the best preliminary final design.
Figure 36 shows the stress distributions at the back and the front of the posterior strut with a SF of 1.5. The red region with a high stress at the top of the posterior strut should be ignored because the force was applied at that point to properly replicate the linear deformation of the AFO during use. Creating this simplification in the FEA simulation develops localized stress, whereas in reality the force is spread throughout the tibial region, which takes away the high stress concentration at the top of the posterior strut.
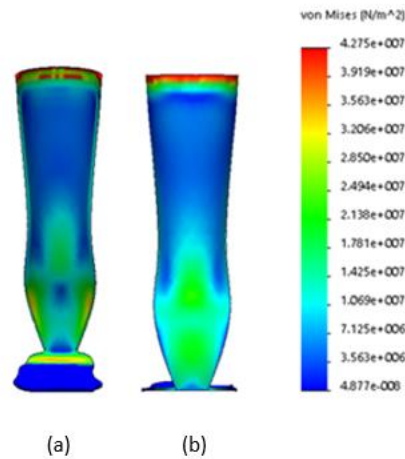
Figure 36. Stress distributions at the a) front and b) back of the posterior strut
from the original model with no fillet and SF of 1.5

Moreover, the sole was thickened so that it does not shear at the metatarsal bone as the patient pushes off the ground and the high stresses at the joint of the posterior strut and the sole were avoided. The sole was increased from 2.5mm to 3mm to accommodate both of these design needs. The posterior strut was thickened along the stiffest portion of the AFO in order get the maximum spring back force while keeping in mind the shoe size of the patient. The patient's shoe is a male size 9.5, which is 275 mm along the inside sole of a typical running shoe [41], In addition to the length of the inside sole, a shoe has a small curve for the heel bone to slide in and fit into, therefore the total length inside a shoe varies from brand to brand and would be bigger than the base of 275mm for a 9.5 shoe size. The increase in thickness of the posterior strut was constrained by the total length of the AFO from the front of the sole to the back of the heel area of the posterior strut, this length was maximized to 275mm, to ensure the brace would fit within the shoe and still have additional space for the patient's comfort. TABLE XVIII shows the optimization of the Basic (PC-ISO, 90°) by thickening the material as required to get the maximum spring back force.

TABLE XVIII
SUMMARY OF THE SOLE AND POSTERIOR STRUT THICKNESS, LENGTH OF THE
BRACE TO FIT IN THE SHOE AND THE SPRING BACK FORCE THE PATIENT GETS
AFTER WEARING THE BRACE

Sole thickness	Increased Posterior strut thickness	Length to fit in the shoe	Spring back force
3mm	1mm	273.45	153
3mm	2mm	274.22	159
3mm	*3mm*	*274.92*	*168*
3mm	4mm	275.83	172

A sole thickness of 3 mm and an increased posterior strut thickness of 3 mm, as shown in TABLE XVIII, was chosen as the optimal thickness to fit within the patient's shoe and which would provide a spring-back force of 168 N. Figure 37 shows the FEA results simulated in SolidWorks® of the optimized Basic (PC-ISO, 90°) design which would fit into the patient's shoe without causing any irritation. A final sole thickness of 3 mm and an increased posterior strut thickness of 3 mm was chosen as the best design to fit within the patient's shoe and provide a spring-back force of 168 N.
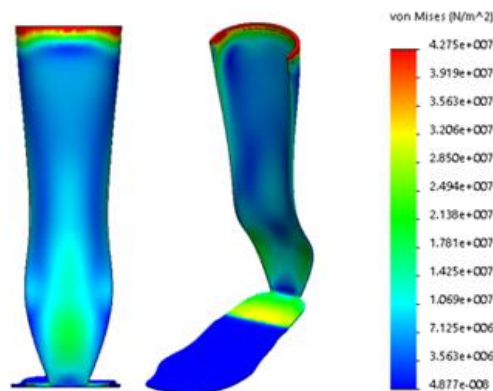
Figure 37. FEA results of optimized Basic (PC-ISO, 90°) design at a 70°stance.

The FEA results of optimized Basic (PC-ISO, 90°) design at a 70° stance showed reduced stress distribution at SF of 1.5, as shown in Figure 37, compared to high

stress distribution at the back of the posterior strut, shown in Figure 36 on page 54. This optimization of thickness showed an improvement in the stress distribution over the posterior strut and sole.

4.3.4 FEA RESULTS

The following sections deal with the final geometric constraints, mesh size setup and the FEA results for preliminary final model of the Basic (PC-ISO, 90°). The FEA test were conducted to determine how each of the models reacted when the posterior strut was bend at 85°, 80°, 75° and 70° angles as the heel pops off the ground, where the areas of high stress formed and the number of iterations of different mesh sizes to achieve the convergence plots. It also includes a supplementary analysis on the comparison with COTS in order to validate the needs of the client.

4.3.4.1 GEOMETRIC CONSTRAINTS

The following summarizes the most optimal geometry that the model was constrained in SolidWorks to simulate the stresses that the AFO would endure during the gait cycle. Additionally, the stress results of the AFO through the gait cycle are presented to validate the durability of the brace.

Fixture

The boundary conditions set for the final FEA was the sole fixed at 2/3 to simulate when the posterior strut bends at 85°, 80°, 75° and 70° angles as the heel pops off the ground. Additionally, the sole was fixed ⅓ along the sole to simulate when the foot reaches the point of pushing off the ground, considered the point of toe-off. The angle between the sole and the posterior strut at toe-off was simulated at 75°. Figure 38 and Figure 39 shows the boundary conditions that were applied to the design.
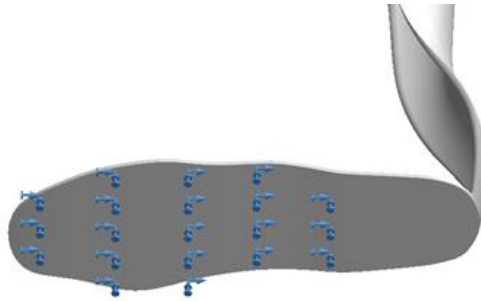
Figure 38. 2/3 of the sole fixed as a geometric constraint in the final FEA simulation.
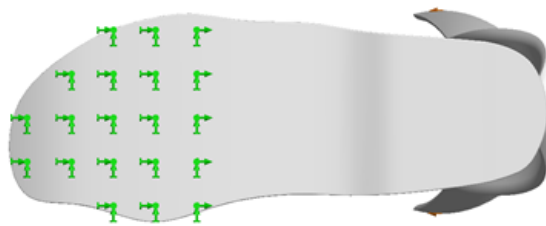
Figure 39. 1/3 of the sole fixed as a geometric constraint in the final FEA simulation

The geometric constraint shown in Figure 38 and Figure 39 were applied to the Basic (PC-ISO, 90°) model for FEA in order the simulate the movement of gait cycle as the heel pops up from the ground.

Meshing

In order to perform the FEA analysis, SolidWorks® requires that mesh be applied to the design. A series of iterations was performed to obtain the convergence plots. Figure 40 and 41 show the two cases with different mesh sizes before the FEA test.
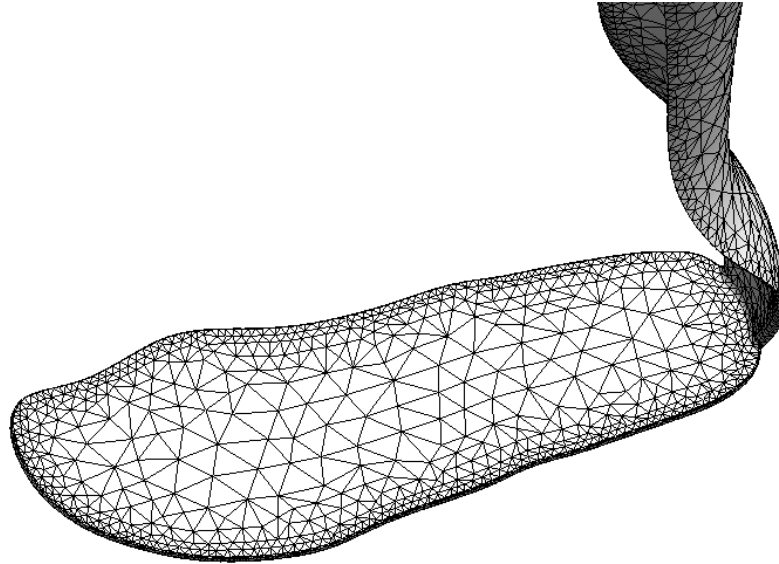
Figure 40. Mesh size of 13mm of the Basic (PC-ISO, 90°) model used in curvature based mesh.
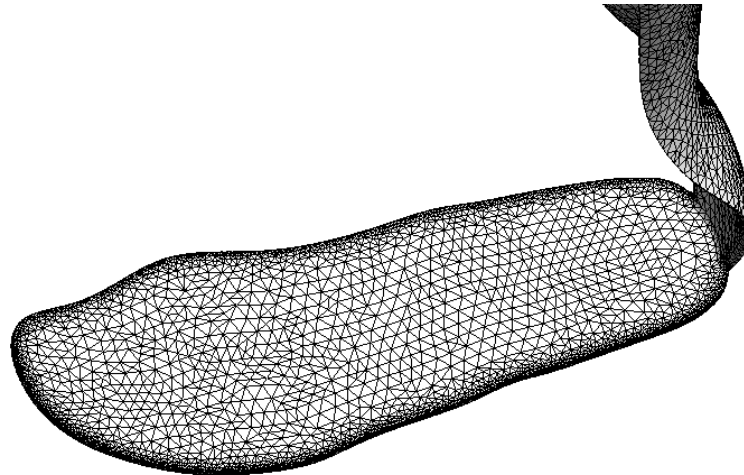
Figure 41. Mesh of the Basic (PC-ISO, 90°). A mesh size of 5mm after 7 iterations was used in curvature based mesh to obtain the convergence plot.

Mesh size of 13 is a case of coarse mesh size as compared to mesh size of 5 which is a case of more refined mesh, as shown in Figure 40 and 41. A series of iterations was performed in FEA with mesh sizes ranging from 13 to 5 used in curvature-based mesh and the result was plotted in Microsoft Excel to obtain the convergence plots, as shown in Figure 42.
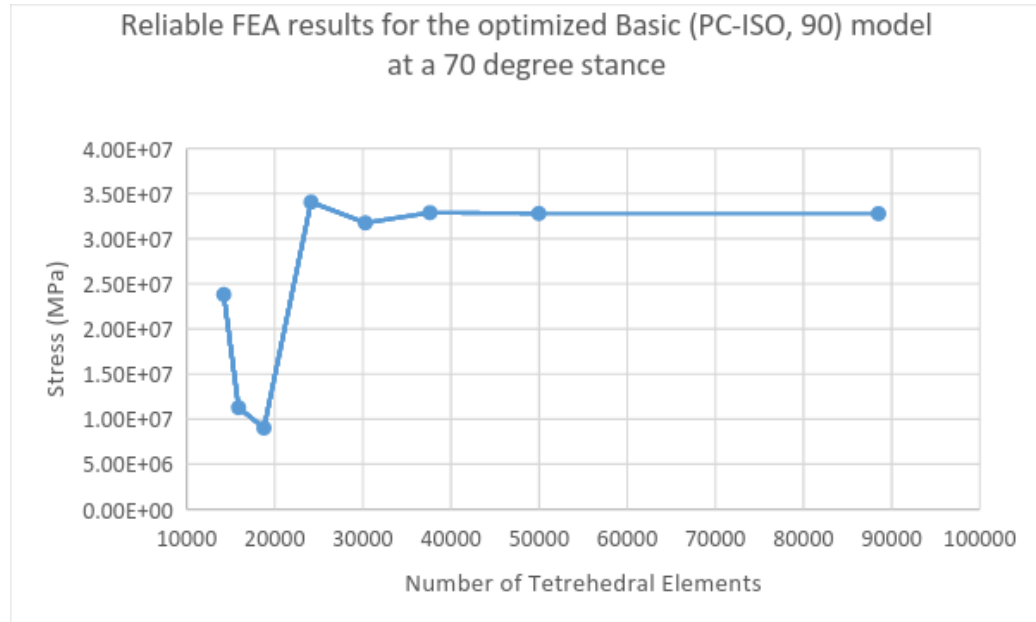
Figure 42. FEA results give the convergence plot of the Basic (PC-ISO, 90°) model at a 70° stance.

Figure 42 compares number of tetrahedral elements versus the maximum stress at the same location on the model by performing multiple iterations of FEA to obtain the convergence plot at a 70° stance. Convergence plots of optimized Basic (PC-ISO, 90°) model with the posterior strut bend at 85°, 80°, and 75° angles are given in Appendix B.

Final model FEA results

TABLE XIX summarizes the FEA results obtained through FEA simulation in SolidWorks®. Stress was increased as the angle between the sole and the posterior strut was increased. Stresses can be seen at the sole and at the posterior strut in TABLE XIX.

TABLE XIX
SUMMARY OF FEA RESULTS OF STRESS DISTRIBUTIONS AT DIFFERENT BEND
ANGLES OF OPTIMIZED BASIC (PC-ISO, 90) MODEL
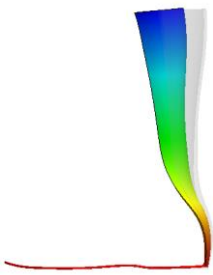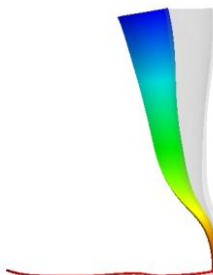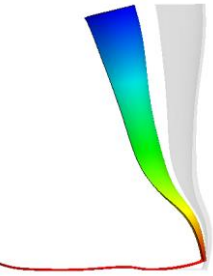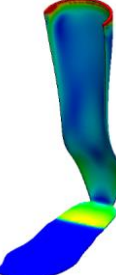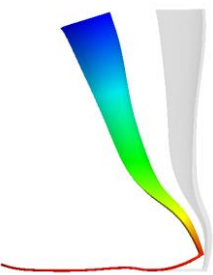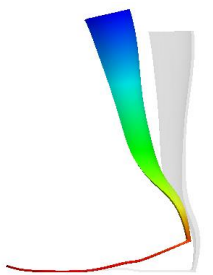
Summary	Stress Distribution (Back)	Stress Distribution (Front)	Deformed Result
Displacement angle: 5° Max Stress = 5.17 MPa Spring -back force = 7.04 N SF = 11.02			
Displacement angle: 10° Max Stress = 11.3 MPa Spring-back force = 31 N SF = 5.04			
Displacement angle: 15° Max Stress = 17.3 MPa Spring-back force = 79.8 N SF = 3.3			
Displacement angle: 20° Max Stress = 32.7 MPa Spring-back force = 161 N SF = 1.74			
Displacement angle: 15° (toe off) Max Stress = 14.3 MPa Spring-back force = 59.9 N SF = 3.98			

Figure 43 also shows the initial position and the maximum displacement of each of the Basic (PC-ISO, 90°) model. The color gradient shows the range of displacement, blue showing the maximum and red being the minimum displacement. Figure 43 shows the final render of the final model.

(a)   (b)

(c)   (d)
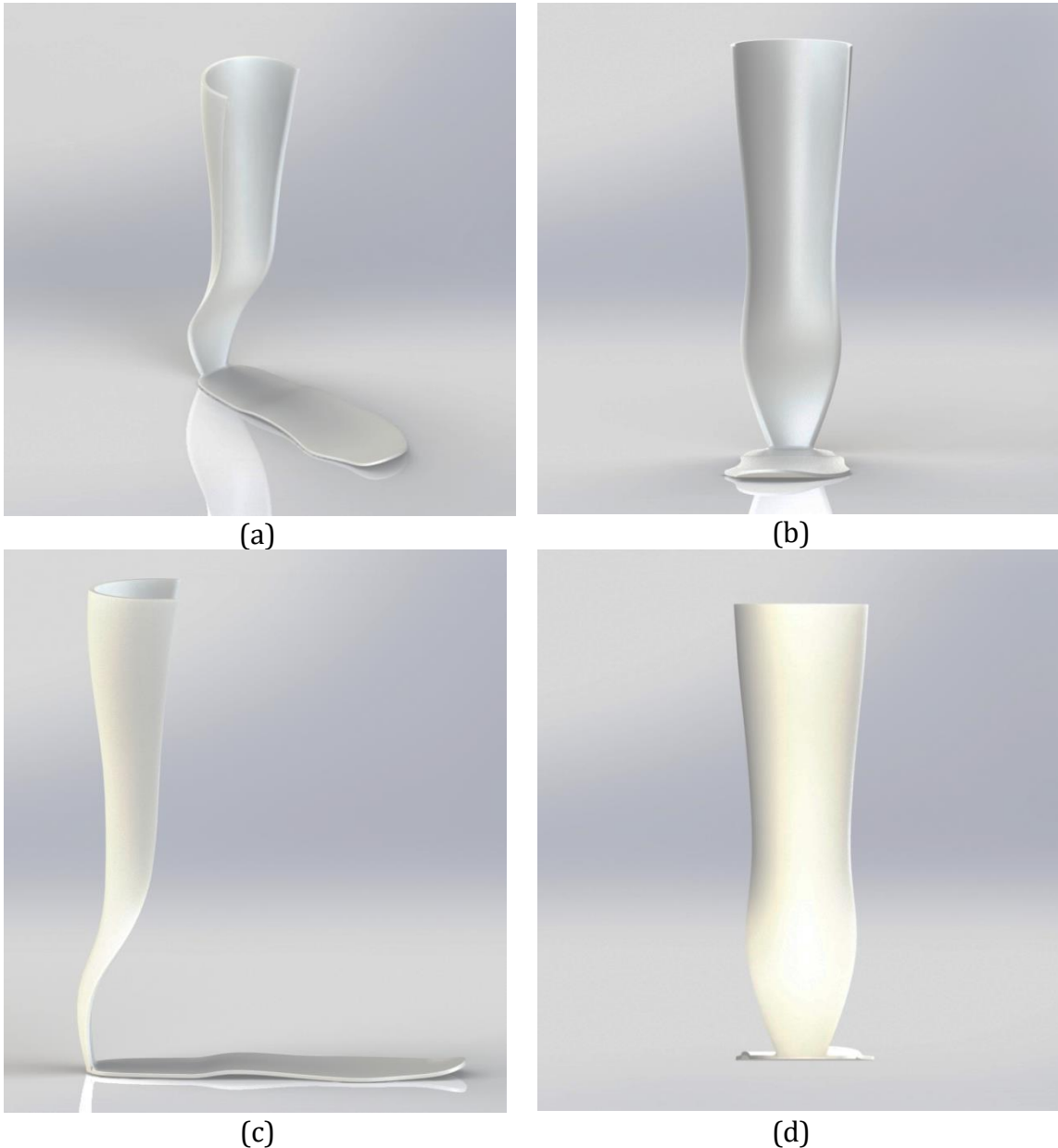
Figure 43. Renders of the final model shows (a) isometric view, (b) front view, (c) side view and (d) rear view.

Supplementary Analysis

To validate that the needs of the client was satisfied, the spring-back force of the final model was compared to the COTS model. This provided quantitative proof that the final design provides an increase in forward propulsion. The COTS model was chosen as the comparison model, since it was used as the benchmark model during the concept screening and scoring, and the preliminary optimization sections. To compare the spring-back forces, an approximate design of the COTS was modeled in SolidWorks® and the same FEA parameters were applied. When the FEA was performed the spring-back force of the COTS was 121N. This lower value proves that the final model designed provides a 38% increase in forward propulsion.

4.3.5 Summary of the Final Model optimization

The Basic (PC-ISO, 90°) was optimized to have a posterior strut thickness of 7 mm and a sole thickness of 3 mm. The final model was optimized through FEA simulations. The boundary conditions of the sole were changed from 2/3 fixed and 1/3 slider roller to only 2/3 fixed for the posterior strut bending at 85°, 80°, 75° and 70° angles and 1/3 fixed for the posterior strut bending at 75° for the best representation of the foot pushing off the ground. Due to the limitation of SolidWorks®, a fillet at the top of the posterior strut induced high stress along the back of the posterior strut, which was an inaccurate representation as the stresses were removed when the fillet was removed. The SF was changed from 2 to 1.5 in order to avoid bulkiness. Also, the SF of 2 was considered to be over constraining the design at the 70° angle, therefore the SF was changed to 1.5 to avoid the possibility of a fracture failure at the joint of the posterior strut and the sole. With the change in the SF and the thickness optimization made to the sole and the posterior strut was implemented the results of FEA estimated the final model would be able to provide a maximum spring-back force of 168N with a SF of 1.74. In order to validate the needs of the client, the spring-back force of the final model was compared to the COTS model. The FEA result of the COTS showed that the final model designed provides a 38% increase in forward propulsion.

5.0 MANUFACTURING

One of the deliverables required by the team for the project was to 3D print our final design in order to verify that the AFO met the client needs and receive patient feedback. The following section presents the processed followed to find a 3D printing facility in Winnipeg, manufacture the brace, and define the cost breakdown for the client.

5.1 North Forge and Precision ADM

The first step to manufacturing the BIA was to research the services offered by North Forge, a 3D printing company in Winnipeg that was recommended by the client. Once the team learned that the North Forge Fabrication Lab held weekly Open Houses, a visit to the facilities was organized. At the Open House, the team inquired about the various 3D printers available, approximate print time and cost, as well as the associated membership cost required to have full access to the machines. In order to move forward, the different options were discussed with the client. The most optimal option for cost and time was to hire one of the 3D printing specialists at North Forge to manufacture the BIA. This option was the most optimal because the team would be able to receive feedback and advice throughout the manufacturing process, reduce the amount of errors, and eliminate the need to purchase a membership at North Forge.

Although North Forge provided the 3D printer, the Fortus 400mc, the material chosen by the team for the final design, PC-ISO, was not available. As a result, Precision ADM an advanced digital manufacturing company in Winnipeg was contacted to provide the required PC-ISO and support material for 3D printing.

5.2 Process

One of the benefits to 3D printing is that the model can be printed in a wide range of orientations, so it was important to determine the orientation that the final model was printed in. Additionally, there were also a few sources of error associated with

3D printing the brace. The following section discusses the printed orientation of the final model, as well as the support material required to build an accurate model.

5.2.1 Printing Orientation

Due to the nature of how the material is layered during 3D printing, the section of the brace printed parallel to the bed would be the less likely to fracture, and the section of the brace printed vertically would be more likely to fracture. Therefore, printing the AFO either upright (sole parallel to the bed) or laying down (posterior strut parallel to the bed) would strengthen the section parallel to the bed, and weaken the section printed vertically. In order to optimize the strength of the sole and posterior strut, the team decided to print the final design at an angle of 19°.

The angle of the sole from the bed was chosen to be 19° due to the limitation of the printing volume in the Fortus 400mc. Initially, the final design was to be printed in an orientation where the sole was inclined at an angle of 20° from the bed, but due to the capacity of the Fortus 400mc, the model would no longer fit in the 3D printer at that angle. As a result, the angle was reduced by one degree so the brace could fit within the capacity of the printer.

5.2.2 Support Material

When printing models with complex shapes and orientations using 3D printers, support material is used to produce a more accurately replicated physical model of the design. Support material provides a surface for the desired material to be printed on, which prevents "drooping" of the material layers . Since the final design was printed an angle, a significant amount of support material to create an angled surface that would allow the brace to be printed at an orientation of 19°, as shown in Figure 44.

Figure 44. a) Close up picture of the sole and b) the final 3D printed model, taken from the side, with the support material attached [41].

The support material can be differentiated from the PC-ISO by observing the surfaces of each material, as shown in Figure 44. The support material, which is a slightly darker shade of white, has a rough surface texture, while the PC-ISO (the thin white layer on top of the support material) is a lighter shade of white and has a smoother surface texture. There were two methods that could have been used to remove the support material after 3D printing: dissolving the support material by submerging the entire model in a liquid solution for around seven hours, or manually chipping away the support material off the PC-ISO.

The 3D printing specialist at North Forge found that it was not possible to submerge the printed model in the specific solution to dissolve the support material because the model floated, and therefore, it was required to manually chip the support material off.

Figure 45. The 3D printed model, taken from the side, after the support material was removed [41].

Once the support material was removed from the 3D printed model, as shown in Figure 45, the model was ready tested by the patient.

5.3 Cost Breakdown

The initial budget for the project was $700, which included the material and labour costs of 3D printing. TABLE XX shows the actual costs of the 3D printing processes required to manufacture the BIA and samples for material testing, and which were compared to the initial budget defined by the client.

TABLE XX
COST BREAKDOWN OF THE MANUFACTURING PROCESS COMPARED TO THE INITIAL PROJECT BUDGET

		Unit Cost	Number of Units	Cost	Budget
Precision ADM	**PC-ISO**	$7/in^3	17.6 in^3	$123.2	$600
	Support Material	$7/in^3	8.8 in^3	$61.60	
North Forge	**Machine Preparation**	$30	1	$30	$100
	Labour	$25/bed	2	$50	
			Total Cost	$264.80	$700

6.0 TESTING

The following sections discusses the testing of the BIA and COTS AFO with the patient in order to gain valuable feedback regarding the performance and stability. This will help in discussion of recommendations of the final model. It also discusses the comparison between fracture strength and maximum stresses in the model at the maximum displacement of 20° where the maximum stress of PC-ISO material was determined in the lab using tensile testing apparatus.

6.1 Testing the BIA

The BIA was tested on the patient under the supervision of our client. Initially the patient walked without a brace, so that the team could differentiate the difference between walking with and without the brace. Some additional changes were made to the BIA before testing on the patient, in order to perform the test accurately. A Velcro was added to the BIA, as shown in Figure 46, so that it can be strapped around the patient's leg.

Figure 46. Velcro fitted on the BIA after 3D printing and before patient testing.

Velcro provides support and comfort when strapped around the patient's leg, shown in Figure 46. Some issues were found during the test. The BIA was not able to fit inside the patient's shoe because the shape of the shoe was not taken into consideration during the design phase, shown in Figure 47.

65

Figure 47.The BIA inside the patient's shoe.

The BIA was bend towards the front due to the inclined shape of the back of the shoe, shown in Figure 47. Since, the BIA was bend forward, it was hard to fit the sole inside the shoe easily and the sole of the BIA sticks out due to the narrow shape design of the shoe. In order to solve this problem, the sole of the BIA was shaved off to the inner size of the shoe. Also, to provide comfort on the sole, a foam was added as shown in Figure 48.

(a)   (b)
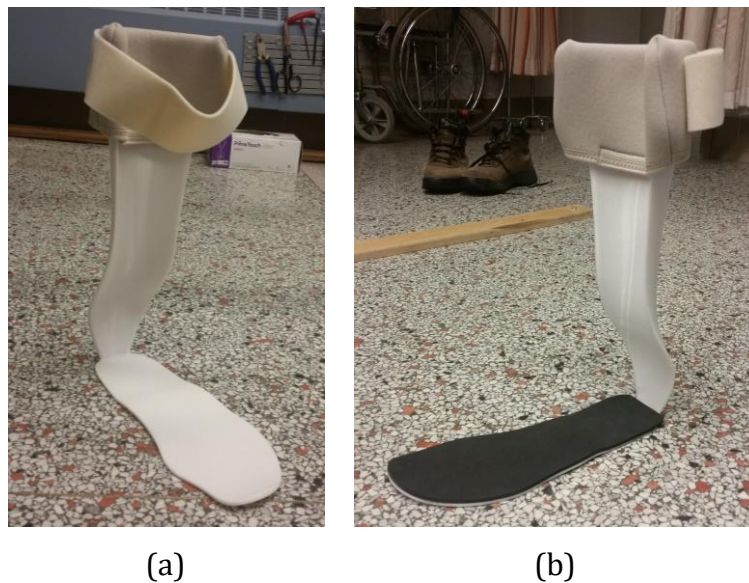
Figure 48. a) The BIA with a sole shape of the inside shoe and b) the pelite foam applied on top of it to provide comfort.

The finished BIA which would be tested is shown in Figure 43. Figure 49 shows patient trying the BIA on.

Figure 49. Patient wearing the BIA at AO.

The patient wore the BIA comfortably, shown Figure 49, and was ready for the test. The patient did a series of test as shown in Figure 50 and Figure 51to analyze the performance of the BIA.
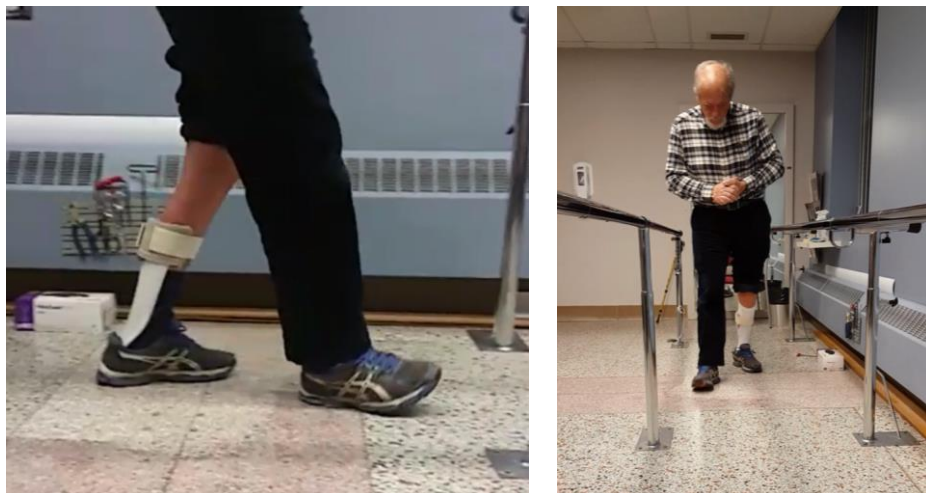
Figure 50. Side and front view of the BIA test on a flat surface.
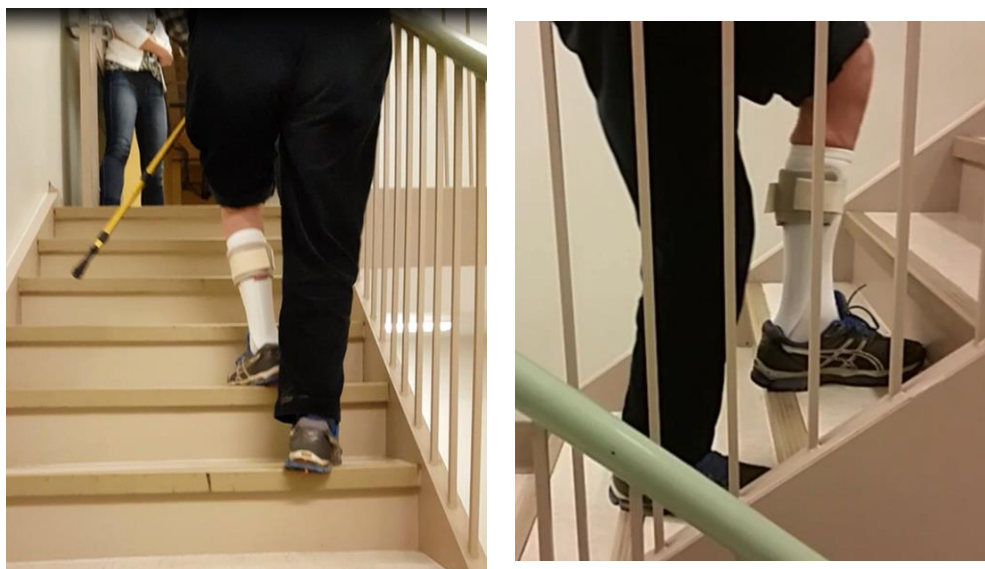
Figure 51. Rear and side view of the BIA test on the staircase.

The patient walked straight on the flat floor and on the staircase, shown in Figure 50 and Figure 51, a number of times back and forth to test the performce of the BIA. The performance of forward propulsion from the BIA, comfortability and any other issues compared to walking without the brace was inquired from the patient.

Additional Testing of COTS

A similar test of COTS was performed with the patient to compare with our design, as shown in Figure 52.

Figure 52. Side view and rear view of the test of COTS on the patient.

The patient walked straight on the flat floor, as shown in Figure 52, a number of times back and forth to test the performce of the COTS and provide a valuable feedback on the performance of the propulsion from the posterior strut, comfortability, weight and aesthetics. The feedback was well recorded.at every step of the test.

6.1.1 Patient feedback

The patient provided a lot of valuable feedback regarding the BIA during and after the test to the team. The following feedback from the patient was documented:

i) The patient was able to lift his leg nicely and there was good toe clearance from the ground

ii) The posterior strut moving could be felt up and down the back of the patient's leg and created friction, but discomfort was reduced by wearing a longer sock

iii) Walking felt natural while wearing the BIA

iv) The BIA did not require the patient to compensate in his other foot as much

v) The patient could feel the spring-back force from the BIA and it felt smooth

vi) The patient did not feel he had to work as hard when walking because the BIA gave more range of motion to his leg, also making him feel more confident and stable

vii) The patient felt that the fitting of the BIA outweighed the weight compared to his current AFO, the BlueROCKER®

viii) The BIA felt tight at the heel and some redness was seen after removing the sock, therefore, an improvement to make note of in that area

The patient also gave a feedback on the COTS AFO. Since the COTS AFO has holes around the heel, it was more comfortable in that area compared to the BIA. The patient was unable to comment on the difference in stability or support provided, but he preferred the BIA over the COTS AFO as it was custom made and it spread around his leg more uniformly. The feedback from the patient allowed the team to make recommendations to improve the design for future testing of the BIA.

6.1.2 Client feedback

After performing the test on the patient, there were some valuable feedback from our client and recommendations to further improve the design. The following feedback from the client was documented:

   i)   Feels that test was a success

   ii)   The BIA was able to provide stability and stance

   iii) An improved progression between the light stance and take off of the leg

   iv)   Overall improvement in gait cycle

   v)   Although, BIA was heavier than the COTS AFO, the client felt that the benefits of function outweighed aesthetics.

The following recommendations for the client was documented:

   i)   Increase in lateral support

   ii)   Width of posterior strut near the heel should be decreased to make it easier to fit into the shoe

   iii) Add more clearance at the heel region instead of foam to decrease discomfort

   iv)   More customized to the shape of the shoe as well as the patient's foot

The feedbacks from the client allowed the team to reflect on the design of the BIA and recommend some design analysis test to be analysed.

6.2 Material Testing

A tensile test is a material behavior analysis that is commonly used to determine the yield, fracture, and ultimate strength of a material using its stress-strain curve. A tensile tester apparatus is used for these tests, shown in Figure 53 a), where a dog bone sample is inserted between the two grips, as shown in below Figure 53b). The top grip slowly applies a tensile force until the sample fractures. The change in the length of the sample (elongation) is measured using a linear extensometer attached to the middle of the sample during the test.

a)   b)
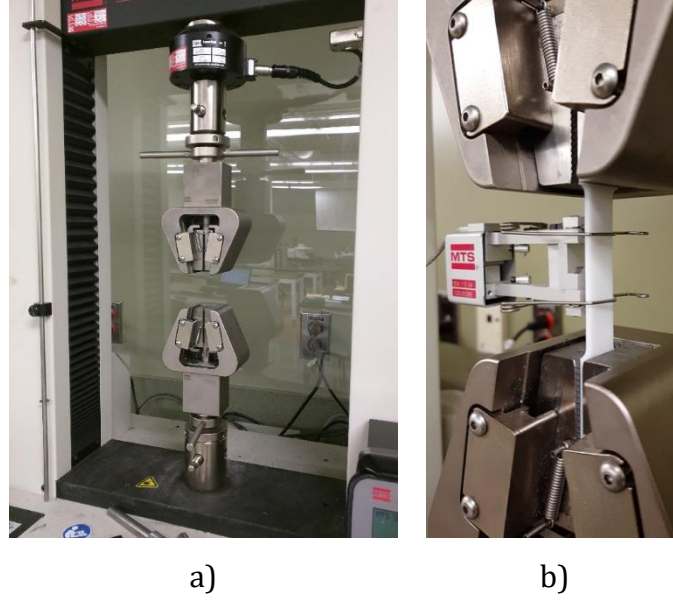
Figure 53. a) MTS Tensile Tester and b) PC-ISO sample mounted between the two grips of the apparatus before testing [42].

The bottom grip remains stationary throughout the test, but as the top grip pulls the sample upwards, the applied force and elongation data is plotted in a load applied versus sample elongation curve. The load and elongation data can then be exported to Microsoft Excel to plot the stress vs. strain curve. The stress and strain for each data sample is calculated using equation (16) and equation (17), respectively.

$$\sigma = \frac{Force}{Initial\ Area} = \frac{F}{A_O} \tag{16}$$

$$\varepsilon = \frac{Final\ Length - Initial\ Length}{Initial\ Length} = \frac{L - L_O}{L_O} \tag{17}$$

The initial area in equation (16) is the cross-sectional area at the center of the sample before testing.

6.2.1 PC-ISO Test Results

The following section presents the orientation of the 3D printing layers of the section of the brace that the dog bone samples represented, and the dimensions of the dog bone samples used to conduct the experiment. The results of the tensile tests performed on the dog bones and the outcome of the results.

Sole (19˚)

The orientation of the material layers at 19°, imitating the sole of the 3D printed BIA is illustrated in red in Figure 54.
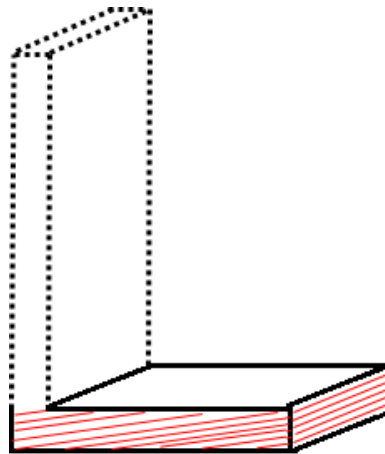
Figure 54. Orientation of the 3D printing material layers at 19°, imitating the sole of the 3D printed BIA.

The dimensions of the horizontal sample printed at 19° are shown in Figure 55.
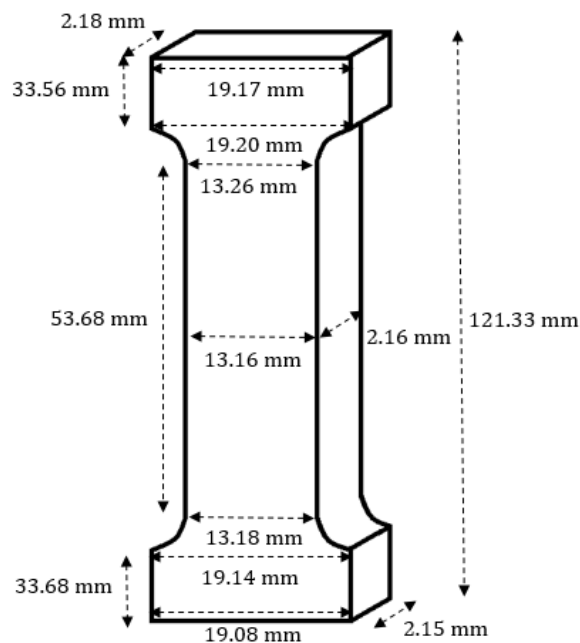
Figure 55. Dimensions of the dog bone when 3D printed at 19°.

The stress-strain curve of the PC-ISO dog bone sample 3D printed at 19°, produced during testing is shown in Figure 56.
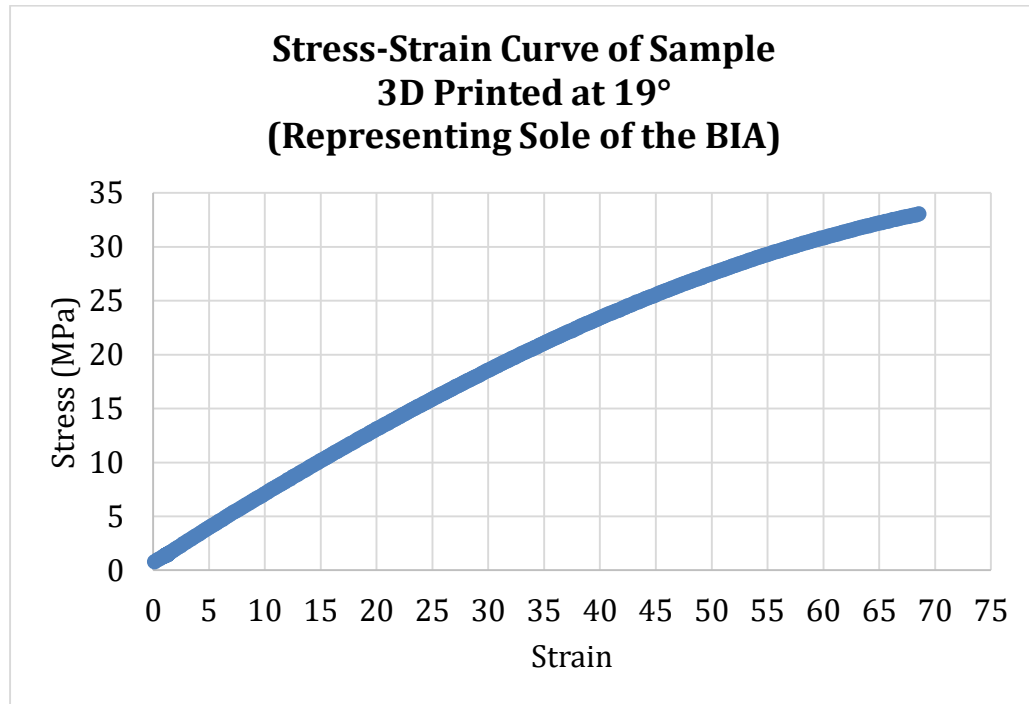
Figure 56. Stress-strain curve of the dog bone sample 3D printed 19°, representing the sole of the 3D printed BIA.

Posterior Strut (71°)

The orientation of the material layers at 71, imitating the posterior strut of the 3D printed BIA is illustrated in red in Figure 57.
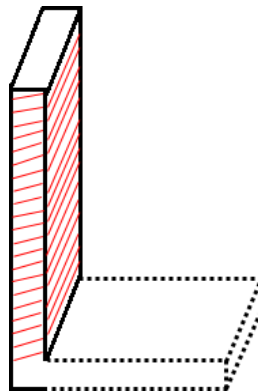
Figure 57. Orientation of the 3D printing material layers at 71°, imitating the posterior strut of the 3D printed BIA.

The dimensions of the horizontal sample printed at 71° are shown in Figure 58.
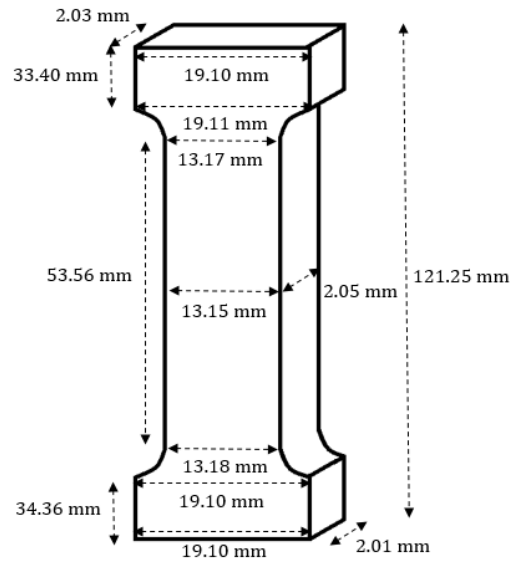
Figure 58. Dimensions of the dog bone when 3D printed at 71°.

The stress-strain curve of the PC-ISO dog bone sample 3D printed at 71°, produced during testing is shown in Figure 59.
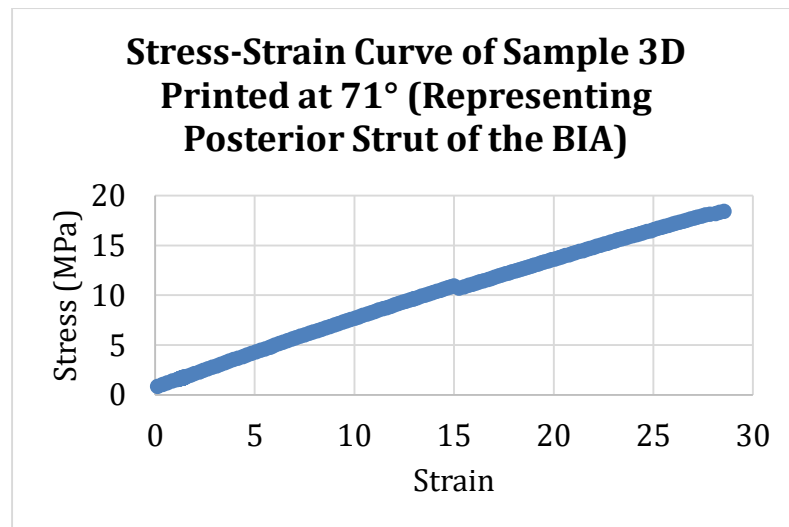
Figure 59. Stress-strain curve of the dog bone sample 3D printed 71°, representing the posterior strut of the 3D printed BIA.

All of the samples tested were brittle, as seen by the highly linear behaviour of the stress-strain curves shown in Figure 56 and Figure 59. The fracture strength is the stress that the material can sustain prior to its sudden failure. An orientation of 19° with respect to the horizontal axis results in a fracture strength of 33.0 MPa for the sole of the BIA, and an orientation of 71°, with respect to the horizontal axis, results in a fracture strength of 18.2 MPa for the posterior strut of the BIA.

Design Validation

To validate the FEA results performed on the final model, the fracture strength of the test specimens was compared to the maximum stresses in the model at the maximum displacement of 20°. The maximum FEA stress along the sole was 32.7 MPa and the maximum FEA stress along the posterior strut was 19.65 MPa. The maximum FEA sole stress is just below the 33.0 MPa fracture strength of the sole test specimen and the maximum FEA posterior strut stress is just above the 18.2 MPa fracture strength of the posterior strut test specimen.

Based on the FEA stresses along the posterior strut, the model would have been predicted to fail by fracture when compared to the tensile strength test results. However, since the BIA had already been tested on the patient, it was known that the AFO would not fracture at the maximum displacement. The results of the tensile strength tests and the results from the patient testing are the most accurate results from the three model analyses. Therefore, the FEA stress results could no longer be considered valid.

The discrepancies from the FEA results and the tensile strength test results could have arisen by the limitations of SolidWorks and the parameters that were set up in the FEA model. The parameters set in FEA may have constrained the model from performing as realistically as possible, which in turn produced higher stresses than what were actually developed during the physical tests. Although the FEA results are not as accurate as expected, the relationship between the force and the stress are still linear. Therefore, the expected value of the spring-back force would be slightly lower than predicted as the stresses the BIA are developing are lower than

the fracture stress from the tensile tests. Section 7.0 contains further detail regarding the limitations of SolidWorks and different methods that could be analyzed to ensure the predicted FEA stress values and applied force results are more accurate.

7.0 RECOMMENDATIONS

The following section discusses the key recommendations that have emerged by working on this project in hope that these can be taken forward by the Anderson Orthopedics in order to improve the design. The following section includes the limitations of using FEA simulation in SolidWorks® compared ANSYS or Abaqus FEA which would provide more accurate results, and Failure Modes and Effects Analysis (**FMEA)** to mitigate the risk in the early development of the BIA.

7.1 Limitations of SolidWorks® FEA Simulation

There are limitations of using FEA simulation in SolidWorks® compared to ANSYS or Abaqus FEA. The FEA results of SolidWorks® is not reliable as seen from the yield test of the dog bone specimen of PC-ISO. SolidWorks® should only be used to prove the physical test. There are lots of discrepancies with the test results of SolidWorks. Unlike SolidWorks, Abaqus FEA specializes in highly nonlinear analysis situations, and can offer a solution to problems that SolidWorks Simulation is unable to perform [43]. It can handle situations with very large amounts of nonlinear deformations or complex behavior. SolidWorks Simulation is good for running early-stage stress analysis with limited loading and restraint options on a single-body part file. SolidWorks only considers movement in one direction and does not consider buckling and other degrees of freedom.

7.2 Failure Modes and Effects Analysis (FMEA)

As a further recommendation, FMEA was performed to mitigate the risks which might occur during use of the BIA. FMEA is a qualitative and systematic tool for analyzing potential reliability problems early in the development cycle where it is easier to take actions and mitigate failure thereby increasing the quality and reliability of the design [44]. FMEA is a structured approach to identifying the ways in which a product or process can fail. It estimates the risk associated with specific

causes and prioritizes the actions that should be taken to reduce the risk. FMEA is also an approach to evaluating the design validation plan and/or the current process control plan.

The basic steps to conduct FMEA for the final design as follows:

i) Identify the components and associated functions that needs to be evaluated.

ii) Identify the potential failure mode(s) that describes the way in which a design fails to perform as intended or according to specification.

iii) Identify the effect or the impact on the customer resulting from the failure mode.

iv) Determine the severity of the failure mode that could impact the design. Establish a numerical ranking 1 representing no effect and to 10 representing severe failure without warning for the severity of the effect as shown in TABLE XXI

v) Identify the causes or means by which an element of the design may result in a failure.

vi) Determine the probability that a given cause or failure mode will occur. Establish a numerical ranking for the likelihood of occurrence. A common scale uses a value of 1 to represent unlikely and 10 to indicate in evitable as shown in TABLE XXII

vii) Identify the controls that are currently in place to either prevent the cause of the failure mode from occurring or detect the failure before it reaches the client.

viii) Determine the likelihood of detection where the likelihood that the current controls placed in the design or process will detect the cause of the failure mode. Establish a numerical scale from 1 representing almost certain and to 10 representing absolute uncertainty as shown in TABLE XXIII

ix) Calculate the Risk Priority Numbers (**RPN**) which is a product of Severity, Probability of Occurrence and Detection ratings.

RPN = Severity x Probability of Occurrence x Detection ratings

x) Determine the recommended actions to reduce risk of potential failures that have high RPN.

TABLE XXI
RATING AND DESCRIPTION OF SEVERITY OF FAILURE MODES

Rating	Effect	Description of Rating	
1	None	No effect. The BIA operates as intended.	Negligible
2	Very Minor	Some patients notice defect. The BIA operates as intended. No effect on patient was found.	
3	Minor	The BIA operates as intended. Slight effect on the patient.	
4	Very Low	Patient comfort or convenience is slightly reduced, but with no injury.	
5	Low	Comfort or convenience is severely reduced, but with no patient injury.	
6	Moderate	The BIA is inoperable with no patient injury.	
7	High	Possible temporary minor injury to patient.	Marginal
8	Very High	Transient minor injury to patient with the possibility of further surgical procedures.	
9	Hazardous	Failing of the BIA can possibly contribute to death, severe injury or permanent significant disability in patient.	Critical
10	Irreversible	Failing of the BIA can cause irreversible damage to patient such as organ failure, limb loss, or death.	Catastrophic

The ratings from 1 to 10 is given in the above table with effect and description of severity of each rating besides it. Rating 1 has no effect where the BIA will operate as intended. The rating increases till 10 where the effect is irreversible and the BIA can cause irreversible damage or death to the patient. Rating 1 – 5 has negligible effect, rating 7 – 8 has marginal effect, rating 9 has critical effect and rating 10 has catastrophic effect on the patient.

TABLE XXII
RATING AND DESCRIPTION OF PROBABILITY OF FAILURE MODES OCCURRENCE

Rating	Probability of Occurrence	Description of Rating
1	Improbable	Failure is unlikely to occur in the BIA
2	Remote	Relatively few failures to occur in the BIA
3		
4	Occasional	Occasional failures to occur in the BIA
5		
6	Probable	Repeated failures to occur in the BIA
7		
8	Frequent	Failure is almost inevitable to occur in the BIA
9		
10		

The ratings from 1 to 10 is given in the above Table with effect and description of probability of failure modes occurrence of each rating besides it. Rating 1 has improbable chance of occurrence and the failure is unlikely to occur in the BIA. It increases till rating 10 where it has frequent chance of occurrence and the failure is almost inevitable to occur in the BIA.

TABLE XXIII
RATING AND DESCRIPTION OF DETECTION OF FAILURE MODES

Rating	Probability of Detection	Description of Rating
1	Almost certain	Current controls will almost definitely detect a potential cause of failure and prevent from further failure.
	Very high	Very high chance current controls will detect cause of failure and prevent from further failure.
	High	High chance current controls will detect cause of failure and prevent from further failure.
2	Moderate	Moderate chance current controls will detect cause of failure and notify the patient.
3	Low	Low chance current controls will detect cause of failure and notify the patient.
	Remote	Remote chance current controls will detect cause of failure.
	Absolute	No current control; cannot detect the cause of failure.

The ratings from 1 to 10 is given in the above Table with effect and description of detection of failure modes of each rating besides it. Rating 1 could be almost certain probability of detection and the current controls would almost certainly detect a potential cause of failure and prevent it from further failure. It goes up till rating 3 where it could be absolute probability of detection and no current controls can detect the cause of failure before it occurs.

The description the FMEA of our preliminary design, as shown in TABLE XXIV, consists of design component, failure modes, failure effects, severity, potential causes, probability of occurrence, current controls and detection to calculate RPN and recommended actions which should be taken to mitigate the risks involved with the BIA.

<div align="center">TABLE XXIV</div>
<div align="center">FMEA OF THE FINAL MODEL OF THE BIA</div>

Case Number	Component	Failure Mode	Failure Effects	Severity	Potential Causes	Probability of	Current controls	Detection	RPN	Recommended Actions
1	Sole beneath metatarsal bone	Fracture	Sole of BIA can cut patient	7	Depending on environment, PC-ISO is brittle	5	No current controls to detect	3	105	Fracture testing to figure out when it will fracture
2	Support around heel	Buckling and/or relaxation	BIA loses support around heel	6	BIA can twist in oblique directions and repeatedly stretch pass maximum range of displacement	3	No current controls to detect	3	54	Further FEA analysis required to analyze the buckling load and reduce risk of occurring
3	Support around lower tibia	Thermo-mechanical fatigue failure	Support around lower tibia is not able to support weight of patient	7	PC-ISO is brittle in cold temperatures and posterior strut can break due to repeated loading	6	No current controls to detect	3	126	Thermo-mechanical fatigue failure test required to further mitigate risk.
4	Support around heel	Fatigue failure	BIA cannot support weight around heel and posterior strut lose it shape	6	Inefficacies sometimes in the nozzle of the 3D printer while printing	3	No current controls to detect	3	54	Fatigue failure test required to determine necessary steps required to mitigate risk
5	Support around heel	Brittle fracture	Sharp surfaces can damage to patient's skin and additional muscular or joint harm	8	Unexpected change in direction or impact while walking	2	No current controls to detect	3	48	Further FEA analysis and fracture test to analyze fracture strength and reduce the risk of occurring
6	Sole	Fracture	Functionality of BIA decreases due to lack in support and can hurt patient	5	Micro fracturing from walking directly on ground with BIA; direct contact with contaminants	5	Warnings on package prior to purchasing	3	75	Discuss risk of damage and personal injury, and advise patients to regularly check for cracking

8.0 CONCLUSION

The team's main objective was to design a 3D printable AFO. In addition to the AFO being 3D printable it was also required that the design be able to support an individual with both dorsiflexor and plantarflexor weaknesses, while providing the affected foot forward propulsion. The optimized AFO also had to be comfortable, safe, lightweight, and last for up to two years.

As the main need of the client was to be able to 3D print the final AFO model, the material, and the stress distribution of the final model were evaluated. The second most important need of the client was to have the posterior strut geometry provide the greatest amount of forward propulsion to the affected foot of an individual, to meet this need the geometry and the applied forces on the AFO were evaluated.

BIA was modelled and evaluated to meet the two main needs of the client by initially evaluating the model on a qualitative analysis. The geometry of the Basic, the Wishbone, the Posterior Lattice and Layered Strut concepts were evaluated in SolidWorks FEA to determine which posterior strut could withstand the applied forces the best. The Basic model proved to perform the best under the constrained settings of the gait cycle.

To ensure the greatest amount of spring-back force would be provided by the AFO without having to exert unrealistic forces to the brace, three inclination angles and three 3D printable materials were combined and evaluated using FEA. The mid-range elasticity and high strength of the PC-ISO material and the inclination angle of 90° prevailed as the most optimal combination.

The third main need of the client was to optimize the AFO to a patient. The Basic concept at 90 degrees was further analyzed by modelling the posterior strut and sole to the geometry of the patient. The BIA has a posterior strut optimized to the patient with a varying thickness from 4 to 7 mm, providing a spring-back force of approximately 168N, resulting in an estimated 38% increase in returned energy. Additionally, the sole was thickened to 3mm to prevent injury to the patient and shearing during the push-off phase of the gait cycle.

Within the time frame of the design project the BIA was 3D printed out of PC-ISO and at a 19° printing angle to prevent shearing along the sole of the AFO. The BIA was able to be tested on the patient at Anderson Orthopedics. The combination of the elastic PC-ISO material and the customized geometry allowed for an increase of mobility and added spring-back during the gait cycle.

The team recommends that the material properties of the BIA be further analyzed using a fatigue analysis and a greater tensile strength sample size to better understand the life-cycle of the brace and the fracture strength of the brace. The combination of these two tests will provide the client with quantitative values to validate the durability of the BIA.

The combination of the positive feedback from the client and the patient and the three main needs of the client being met confirms the design approach used to solve AO's main problem was satisfactory.

9.0 REFERENCES

[1] "Orthopedics," [Online]. Available: http://www.merriam-webster.com/ dictionary/orthopedics. [Accessed 26 September 2016].

[2] "Orthosis," [Online]. Available: http://medical-dictionary.thefreedictionary.com/ orthosis. [Accessed 26 September 2016].

[3] "Prosthetic," [Online]. Available: http://www.dictionary.com/browse/prosthetic. [Accessed 26 September 2016].

[4] Anderson Orthopedics. (2014). "Home" [Online]. Available: http://andersonortho.ca/aboutprosthetics-and-orthotics-winnipeg-brandon-manitoba/ [Sept 20, 2016].

[5] Theoi (n.d.). *Bia* [Online]. Available: http://www.theoi.com/Daimon/Bia.html [November 28, 2016].

[6] W. Hadi (private communication), Sept 20,2016.

[7] TeachMeAnatomy. (2016, Aug. 15th). "Anatomical Terms of Movement" [Online]. Available: http://teachmeanatomy.info/the-basics/anatomical-terminology/ terms-of-movement/ [Sept 25, 2016].

[8] R.C. Schafer. (1987). "Body Alignment, Posture and Gait," in Clinical Biomechanics: Musculoskeletal Actions and Reactions, 2nd Edition [Online]. Baltimore, Wiliams & Wilkins, January, Chapter 4. Available: http://www.chiro.org/ACAPress/ Body_Alignment.html [Sept. 25, 2016].

[9] Anderson Orthopedics, "The U of M IDEA Program Application Form," unpublished. [Sept 9, 2016].

[10] "Ankle Foot Drop AFO Brace Orthosis Splint Leaf Spring Recovery Equipment" (n.d.). [Online]. Available: https://www.aliexpress.com/item/Free-shipping-hot-selling-Ankle-foot-drop-brace-orthopedic-shoe-foot-supporting-feet-stroke-hemiplegia-

rehabilitation/1391868588.html?spm=2114.40010708.4.15.qq6mnc
[Sept. 25, 2016].

[11] Somastruct. (2015). "Take off your shoes when stretching calves" [Online].
Available: http://www.somastruct.com/take-off-your-shoes-when-stretching-
your-calves/ [Oct 18, 2016].

[12] Prospector. (2016). "Polypropylene (PP) Typical Properties of Generic PP
Homopolymer" [Online]. Available:
https://plastics.ulprospector.com/generics/
39/c/t/polypropylene-pp-properties-processing/sp/13 [Oct 21, 2016].

[13] North Forge Technology Exchange. (2016). *Equipment/Rooms* [Online].
Available:
https://www.northforge.ca/fabrication-lab/ [October 25, 2016].

[14] 3D Printers Canada. (n.d.). *Objet260 Connex - The First Compact Multi-Material
3D
Printing System* [Online]. Available: http://www.3dprinterscanada.com/
260-connex.php [October 25, 2016].

[15] Stratasys. (2016). *uPrint SE Plus* [Online]. Available:
http://www.stratasys.com/
3d-printers/idea-series/uprint-se-plus [October 25, 2016].

[16] GrabCad. (2016). "3D Scanned Human Legs" [Online]. Available:
https://grabcad.com/library/3d-scanned-human-legs-second-model-1
[Oct 18, 2016].

[17] 3D Hubs. (2016). *3D Printer Overview* [Online]. Available:
https://www.3dhubs.com/3d-printers#professional [October 25, 2016].

[18] Lincoln Machine Inc. (2016, Oct 26th). "Fortus 400mc" [Online]. Available:
http://www.lincolnmachine.com/Fortus-SS-400mc.pdf [Oct 19, 2016].

[19] Sindoh. (n.d.) *3DWOX* [Online]. Available: http://3dprinter.sindoh.com/
Product3Dwox [October 25, 2016].

[20] Stratasys, "FDM Thermoplastics," Stratasys Ltd. , 2016. [Online]. Available:
http://www.stratasys.com/materials/fdm. [November 12, 2016].

[21] Stratasys, "ABSplus," 2016. [Online]. Available:
http://usglobalimages.stratasys.com/Main/Files/Material_Spec_Sheets/
MSS_FDM_ABSplusP430.pdf. [November 9, 2016].

[22] Stratasys, "ABSi," 2016. [Online]. Available: http://usglobalimages.stratasys.com/ Main/Files/Material_Spec_Sheets/MSS_FDM_ABSi.pdf. [Accessed 9 November 2016].

[23] Stratasys, "ABS-M30," 2016. [Online]. Available: http://usglobalimages.stratasys.com/Main/Files/Material_Spec_Sheets/ MSS_FDM_ABSM30.pdf. [Accessed 9 November 2016].

[24] Stratasys, "ABS-M30i," 2016. [Online]. Available: http://usglobalimages.stratasys.com/Main/Files/Material_Spec_Sheets/ MSS_FDM_FortusABSM30i.pdf?v=635784425363214875. [Accessed 9 November 2016].

[25] Stratasys, "ABS-ESD7," 2016. [Online]. Available: http://usglobalimages.stratasys.com/Main/Files/Material_Spec_Sheets/ MSS_FDM_ABSESD7.pdf. [Accessed 9 November 2016].

[26] Stratasys, "ASA," 2016. [Online]. Available: http://www.stratasys.com/~/ media/Main/Files/Material_Spec_Sheets/MSS_FDM_ASA.ashx. [Accessed 9 November 2016].

[27] Stratasys, "Nylon 12," 2016. [Online]. Available: http://usglobalimages.stratasys.com/Main/Files/Material_Spec_Sheets/ MSS_FDM_Nylon12.pdf. [Accessed 9 November 2016].

[28] Stratasys, "PC," 2016. [Online]. Available: http://usglobalimages.stratasys.com/Main/Files/Material_Spec_Sheets/ MSS_FDM_PC.pdf. [Accessed 9 November 2016].

[29 tratasys, "PC-ABS," 2016. [Online]. Available: http://www.stratasys.com/~/ media/Main/Files/Material_Spec_Sheets/ PC_ABS_MaterialSpecSheet_English.pdf?la=en. [Accessed 9 November 2016].

[30] Stratasys, "PC-ISO," 2016. [Online]. Available: http://usglobalimages.stratasys.com/Main/Files/Material_Spec_Sheets/ MSS_FDM_2PCISO.pdf?v=635785194861785354. [Accessed 9 November 2016].

[31] Stratasys, "PPSF," 2016. [Online]. Available: http://usglobalimages.stratasys.com/ Main/Files/Material_Spec_Sheets/MSS_FDM_FortusPPSF.pdf. [Accessed 9 November 2016]

[32] Stratasys, "Ultem 1010," 2016. [Online]. Available:
http://usglobalimages.stratasys.com/Main/Files/Material_Spec_Sheets/
MSS_FDM_ULTEM1010.pdf. [Accessed 9 November 2016].

[33] Stratasys, "Ultem 9085," 2016. [Online]. Available:
http://usglobalimages.stratasys.com/Main/Files/Material_Spec_Sheets/
MSS_FDM_ULTEM9085.pdf. [Accessed 9 November 2016].

[34] Quintic 4 Edudaction, "Q4E Case Studies," Quintic Consultancy Ltd. , 2016.
[Online]. Available: http://www.quintic.com/education/case_studies/
Gait%20Analysis.html. [Accessed 6 November 2016].

[35] Unknown, "Do YOU have long/average/short legs?," Limb Lengthening Forum ,
23 June 2014. [Online]. Available: http://www.limblengtheningforum.com/
index.php?topic=723.0. [Accessed 15 November 2016].

[36] D. M. Harrison, "Forces on the Leg," 24 October 2004. [Online]. Available:
http://www.upscale.utoronto.ca/PVB/Harrison/HipForces/HipForces.html.
[Accessed 15 November 2016].

[37] D. Halls, "Moose and Doc," 15 November 2016. [Online]. Available:
http://halls.md/average-height-men-height-weight/.
[Accessed 15 November 2016].

[38] Wikipedia, "Center of mass," Wikipedia, 15 November 2016. [Online]. Available:
https://en.wikipedia.org/wiki/Center_of_mass. [Accessed 15 November 2016].

[39] M. Borojevic, "Normal and Tangential components of Acceleration,"
23 October 1996. [Online]. Available: http://omega.albany.edu:8008/calc3/
curves3-dir/lecture.html. [Accessed 15 November 2016].

[40] D. S. Essa, "Gait Analysis," 23 December 2012. [Online]. Available:
http://www.slideshare.net/shimaa2022/gait-analysis-15743497.
[Accessed 15 November 2016].

[41] Mens Shoe Sizes. (2014). "Metrication" [Online]. Available:
http://www.metrication.com/clothing/shoes.html [November 23, 2016].

[42] John Hache. "3D Printing the BIA". North Forge Fabrication Lab, Winnipeg, MB,
November 26, 2016

[43] Misilyna Wu. "Tensile Testing". EITC E1-473, University of Manitoba,
Winnipeg, MB, December 1, 2016

[44] Hawk Ridge System, 2014. [Online]. Available: http://www.hawkridgesys.com/ file/solidworks-simulation/Simulation-Buyers-Guide.pdf [Accessed 24 November 2016]

[45] "Failure Modes and Effects Analysis (FMEA)", *Npd-solutions.com*, 2016. [Online]. Available: http://www.npd-solutions.com/fmea.html. [Accessed: 20 Nov 2016].

[46] Johns Hopkins Medicine. (n.d.). *Peroneal Nerve Injury (Foot Drop)* [Online]. Available: http://www.hopkinsmedicine.org/neurology_neurosurgery/centers_clinics/ peripheral_nerve_surgery/conditions/foot_drop_injury.html [November 21, 2016].

[47] Z Corporation. (January 2009). *Z Corporation ZPrinter 650* [Online]. Available: http://zcorp.com/documents/386_2009-0101-DEVELOP3D-650.pdf [October 25, 2016].

APPENDIX